

# Chapter 1

## An Introduction to Astrophysical Black Holes and Their Dynamical Production

Luciano Rezzolla

**Abstract** Astrophysical black-hole candidates provide the most abundant, and possibly the only, evidence of the existence of black holes in nature. These lectures are aimed at providing a basic theoretical introduction to the mathematical properties of astrophysical black holes and to the dynamical processes leading to their formation. In particular, I will first concentrate on the process of gravitational collapse as this will illustrate how an isolated black hole can be produced under rather general physical conditions. Next, I will discuss how the properties of a black hole can be investigated by studying the motion of test particles and the various classes of orbits they follow. Finally, I will consider the process of formation of a black hole from the merger of a binary system of black holes. In particular, I will show that it is possible to predict the mass and spin of the final black hole simply in terms of the properties of the two initial black holes.

### 1.1 Introduction

The investigation of the dynamical processes leading to the formation of an astrophysical black hole has a long history and still represents one of the most interesting and rich problems in general relativity. In this chapter I will present a brief overview of this topic considering two rather different processes, namely, the gravitational collapse to a non-rotating self-gravitating object (either a dust cloud or a star) and the merger of two black holes.

In the first part of this chapter I will show that gravitational collapse can, under suitable conditions, be the inevitable end state of a self-gravitating object. Next, I will illustrate the simplest and yet revealing model of gravitational collapse: the Oppenheimer-Snyder collapse of a dust sphere to a black hole. Special attention will be paid to the dynamics of trapped surfaces, such as apparent and event horizons. I will then turn to the more realistic case of the gravitational collapse of a self-

---

L. Rezzolla (✉)

Institute for Theoretical Physics, Frankfurt am Main, Germany

Frankfurt Institute for Advanced Studies, Frankfurt am Main, Germany

e-mail: [rezzolla@itp.uni-frankfurt.de](mailto:rezzolla@itp.uni-frankfurt.de)

gravitating fluid sphere, exploiting all the insight gained with dust. Once the basic features of the gravitational collapse have been discussed and the idea of black hole introduced, I will briefly discuss how we can learn about the properties of black holes, spherical and axisymmetric, considering the motion of test particles. The second part of the chapter is instead dedicated to a rather different route leading to the formation of an isolated black hole: the merger of a binary of black holes. In particular, I will show how it is possible to compute the mass and spin of the final black hole simply in terms of an algebraic expression containing information on the properties of the two initial black holes.

In the following I will use a spacelike signature  $(-, +, +, +)$  and a system of units in which  $c = G = M_{\odot} = 1$  unless stated otherwise. Four-dimensional covariant and partial derivatives will be indicated in general with  $\nabla_{\mu}$  and  $\partial_{\mu}$ , while vectors (either four or three-dimensional) will be marked with a boldface font. Within the standard convention of a summation of repeated indices, Greek letters will be taken to run from 0 to 3, while Latin indices run from 1 to 3.

A final word before starting is one of caution. It is quite obvious that the topics potentially covered under such a title can be countless, but also that this would not reflect what presented at the School. Hence, the ground covered in this chapter is very limited and aimed at providing the most basic theoretical elements about astrophysical black holes. Additional information on many of the topics covered here can be found in [1–5].

## 1.2 Compact Stars and Black Holes

Within a realistic astrophysical context, any discussion concerning the gravitational collapse to black holes would necessarily start from considering the existence of the “progenitors”, i.e., of stars whose pressure, in the course of their evolution, would fail to balance the gravitational attraction. However, I will not take this step here and, rather, bypass the problem by assuming that it is possible to construct a spherical stellar model compelled to collapse to a black hole.

The indication that this scenario is at least plausible if not realistic comes already from considering the simplest possible example: a spherically-symmetric, uniform density, perfect-fluid star. Before asking about the gravitational collapse and its inevitability in this case, let us recall how to find the equations for a star made by a perfect fluid described by a stress-energy tensor of the type

$$T^{\mu\nu} = (e + p)u^{\mu}u^{\nu} + pg^{\mu\nu}, \quad (1.1)$$

where  $e$ ,  $u^{\mu}$  and  $p$  are, respectively, the total mass-energy density, the fluid four-velocity and the (isotropic) pressure. The conservation of energy-momentum tensor

$$\nabla_{\alpha} T^{\alpha\beta} = 0, \quad (1.2)$$

and of the baryon number density  $n := \rho/m_0$

$$\nabla_\alpha (nu^\alpha) = 0, \quad (1.3)$$

provides the hydrodynamic equations that the stellar configuration has to satisfy. Here,  $m_0$  is the mass of the particles composing the fluid (assuming for simplicity that there is of one kind of particles) and  $\rho$  the rest-mass density. In Eqs. (1.2) and (1.3), the operator  $\nabla$  represents the covariant derivative with respect to the spherically symmetric line-element

$$ds^2 = -e^{2\Phi} dt^2 + e^{2\Lambda} dr^2 + r^2 d\Omega^2, \quad (1.4)$$

where  $d\Omega^2 = d\theta^2 + \sin^2\theta d\phi^2$ . Projecting now Eq. (1.2) in the direction orthogonal to the fluid four-velocity through the projector operator

$$P^{\alpha\beta} = u^\alpha u^\beta + g^{\alpha\beta}. \quad (1.5)$$

we obtain the general relativistic Euler equations

$$(e + p)a_\mu = -P_\mu^\beta \partial_\beta p, \quad (1.6)$$

where  $a_\mu := u^\beta \nabla_\beta u_\mu$  is the fluid four-acceleration. The similarity of Eq. (1.6) with the corresponding Euler equations

$$\rho(\partial_t v^i + v^j \partial_j v^i) = -\partial^i p - \partial^i \Phi_{\text{Newt}}, \quad (1.7)$$

for a fluid with three-velocity  $v^i$  in a Newtonian gravitational potential  $\Phi_{\text{Newt}}$  is rather transparent. Imposing the conditions of stationarity and spherical symmetry, the only remaining non-trivial Euler equation is

$$(e + p) \frac{d\Phi}{dr} = -\frac{dp}{dr}, \quad (1.8)$$

where the metric potential  $\Phi$  is clearly related to the corresponding Newtonian gravitational potential  $\Phi_{\text{Newt}}$ .

Next, we consider the Einstein field equations  $G_{\alpha\beta} = 8\pi T_{\alpha\beta}$  and introduce the following parameterisation of the radial coefficient of the metric

$$g_{rr} := e^{2\Lambda} = \frac{1}{1 - 2m(r)/r}, \quad (1.9)$$

so that

$$m(r) = \frac{1}{2} r (1 - e^{-2\Lambda}). \quad (1.10)$$

The non-zero components of the Einstein tensor are

$$G_{00} = \frac{e^{2\Phi}}{r} [r(1 - e^{-2\Lambda})]', \quad (1.11)$$

$$G_{rr} = -\frac{e^{2\Lambda}}{r} (1 - e^{-2\Lambda}) + \frac{2}{r} \Phi', \quad (1.12)$$

$$G_{\theta\theta} = r^2 e^{-2\Lambda} \left[ \Phi'' - (\Phi')^2 + \frac{\Phi'}{r} - \Phi' \Lambda' - \frac{\Lambda'}{r} \right], \quad (1.13)$$

$$G_{\phi\phi} = G_{\theta\theta} \sin^2 \theta, \quad (1.14)$$

where the prime indicates the radial derivative. The Einstein equations become

$$\frac{dm(r)}{dr} = 4\pi r^2 e, \quad (1.15)$$

$$\frac{dp}{dr} = -\frac{(e+p)(m+4\pi r^3 p)}{r(r-2m)}. \quad (1.16)$$

Equations (1.8), (1.15), (1.16), supplemented by an equation of state relating, say,  $p$  and  $\rho$ , are known as the Tolman, Oppenheimer and Volkoff (TOV) equations. Solving the TOV equations requires, in general, a numerical integration; fortunately, analytic expressions are available in the case of a spherically-symmetric star of uniform density. The radius  $R$  of the star is defined as the locus where the pressure vanishes:  $p(R) = 0$  whereas  $p(r) \neq 0$  for  $r < R$  i.e., in the interior of the star. Recalling that Birkhoff's theorem guarantees that the exterior solution is the Schwarzschild solution [1, 2], one easily deduces that the metric components are given by

$$g_{rr} = \begin{cases} \left(1 - \frac{2}{r} \frac{4\pi r^3}{3} e_0\right)^{-1} & \text{for } r \leq R \text{ (interior),} \\ \left(1 - \frac{2M}{r}\right)^{-1} & \text{for } r > R \text{ (Schwarzschild),} \end{cases} \quad (1.17)$$

and

$$\sqrt{-g_{tt}} = e^\Phi = \begin{cases} \frac{3}{2} \left(1 - \frac{2M}{R}\right)^{1/2} - \frac{1}{2} \left(1 - \frac{2Mr^2}{R^3}\right)^{1/2} & \text{for } r \leq R \text{ (interior),} \\ \left(1 - \frac{2M}{r}\right)^{1/2} & \text{for } r > R \text{ (Schwarzschild).} \end{cases}$$

In the previous expressions,  $M$  is the “gravitational mass” of the star

$$M := \int_0^R 4\pi r^2 e_0 dr = \frac{4\pi}{3} R^3 e_0, \quad (1.18)$$

so that the average energy density is

$$e_0 = \frac{3M}{4\pi R^3}. \quad (1.19)$$

Needless to say, although the density is uniform within the star, the pressure is not and is given by

$$p = p(r) = e_0 \left[ \frac{(1 - 2Mr^2/R^3)^{1/2} - (1 - 2M/R)^{1/2}}{3(1 - 2M/R)^{1/2} - (1 - 2Mr^2/R^3)^{1/2}} \right]. \quad (1.20)$$

For a given choice of  $M$ , the radius  $R$  of the star can be calculated explicitly from the density  $e_0$  and the value of the pressure in the center of the star

$$p_c := p(r = 0) = e_0 \left[ \frac{1 - (1 - 2M/R)^{1/2}}{3(1 - 2M/R)^{1/2} - 1} \right], \quad (1.21)$$

and by imposing the vanishing of the pressure at  $r = R$

$$R = \sqrt{\frac{3}{8\pi e_0} \left[ 1 - \frac{(e_0 + p_c)^2}{(e_0 + 3p_c)^2} \right]}. \quad (1.22)$$

Overall, the uniform-density solution depends on a single parameter  $e_0$ , but has an important limit in the ratio  $M/R$ , which is also referred to as the *compactness* of the star. In particular, Eq. (1.21) indicates that  $p_c \rightarrow \infty$  for  $M/R \rightarrow 4/9$ ; an infinite pressures is therefore necessary to support a star with a radius  $R < 9/8R_S$ , where  $R_S := 2M$  is Schwarzschild radius. As a result, should a star reach such compactness, its final fate can only be that of a black hole. This is sometimes referred to as “Buchdal’s theorem” and applies also to more realistic equations of state.

### 1.3 Oppenheimer-Snyder Collapse

So far we focused on stationary configurations but the gravitational collapse is clearly a dynamical process involving considerable portions of spacetime. Also in this case, it is useful to start studying a simplified scenario as the one offered

by the collapse of a star made of uniform-density pressureless dust. This is also known as the Oppenheimer-Snyder (OS) collapse [6]. In this case, in fact, the fluid motion is particularly simple being that of collisionless particles having a highly symmetric collective motion. In addition, the spherical symmetry (via Birkhoff's theorem) guarantees that the only portion of spacetime that is undergoing an effective evolution is the interior of the star, the exterior always remaining that of a Schwarzschild solution (albeit with a dynamical boundary).

Before looking at the details of the dynamics it is useful to consider the set of equations, both Einstein's and hydrodynamical, that describe the process; these equations are also the starting point for the study of general relativistic cosmology.

We start considering a spherically symmetric, diagonal line element<sup>1</sup> of the form

$$ds^2 = -a^2 dt^2 + b^2 dr^2 + R^2 d\Omega^2. \quad (1.23)$$

where  $a$  and  $b$  are functions of  $(r, t)$ . Here,  $R$  is a circumferential radial coordinate since the proper circumference is calculated simply as

$$\mathcal{C} = \int_{r, \theta = \text{const.}} \sqrt{ds^2} = \int \sqrt{g_{\phi\phi}} d\phi = 2\pi R. \quad (1.24)$$

Adopting a set of comoving coordinates, the fluid four-velocity is  $u^\alpha = (u^0, 0, 0, 0)$ , and since  $u^\alpha u_\alpha = -1$  so that

$$u^\alpha = (a^{-1}, 0, 0, 0), \quad u_\alpha = (-a, 0, 0, 0). \quad (1.25)$$

To cast the hydrodynamic equations in a form that resembles corresponding Newtonian expressions, it is better to introduce differential operators that measure variations with respect to the proper distance and time. In general

$$\frac{\partial}{\partial(\text{proper } x^\beta \text{ coordinate})} = \frac{\partial}{\sqrt{g_{\alpha\beta}} \partial x^\beta}, \quad (1.26)$$

$$D_t = \text{proper time derivative} := \frac{1}{a} \partial_t, \quad (1.27)$$

$$D_r = \text{proper radius derivative} := \frac{1}{b} \partial_r. \quad (1.28)$$

We may introduce the quantities

$$u := D_t R = \frac{1}{a} \partial_t R, \quad \Gamma := D_r R = \frac{1}{b} \partial_r R, \quad (1.29)$$

---

<sup>1</sup>In spherical symmetry there is no loss of generality in doing this choice.

where  $u$  is the radial component of a four-velocity in a coordinate system that has  $R$  as the radial coordinate, while  $\Gamma$  measures the variation of the circumferential radius with respect to the radial coordinate. With the above choices, the full set of equations for the field and for the fluid is written as follows

$$\frac{D_t e}{e+p} = \frac{D_t e_0}{e_0}, \quad (\text{conservation of energy}), \quad (1.30)$$

$$\frac{D_t e_0}{e_0} = -\frac{1}{R^2} \partial_R (u R^2), \quad (\text{conservation of baryon number}), \quad (1.31)$$

$$D_t u = -\frac{\Gamma}{e+p} D_r p - \frac{m}{R^2} - 4\pi p R, \quad (\text{conservation of momentum}), \quad (1.32)$$

$$D_t \Gamma = -\frac{u}{e+p} D_r p, \quad (1.33)$$

$$D_t m = -4\pi R^2 u e, \quad (1.34)$$

$$\Gamma^2 = 1 + u^2 - \frac{2m}{R}. \quad (1.35)$$

The last three equations are the only nonzero Einstein equations and the function  $\Gamma$  represents the general-relativistic analogue of the Lorentz factor of special relativity ( $\Gamma = 1$  in Newtonian physics). Equations (1.30)–(1.35), together with an equation of state, represent the set of equations to be solved to compute the evolution of the interior spacetime of a star that is collapsing.

In the case of dust, the fluid particles are collisionless and share the same radial motion. The pressure vanishes and this simplifies the above set of equations considerably. Furthermore, since the rest-mass does not change during the collapse, we can introduce a new variable that labels the different shells with the rest-mass they contain, i.e.

$$\mu(r) := \int 4\pi R^2 \rho b \, dr. \quad (1.36)$$

Clearly, this parameterisation is valid as long as each shell does not interact with the neighbouring ones, i.e., there is no shell-crossing.

Let us consider now the consequences of the hypothesis that the fluid is *homogeneous*, i.e.,  $D_r p = 0 = D_r e$ . In this case, the first of Eq. (1.34) reduces to  $D_t \Gamma = 0$ , so that  $\Gamma = \Gamma(\mu)$  only and

$$m = \int_0^{R_0} 4\pi R^2 e \, dR = \frac{4\pi}{3} R_0^3 e. \quad (1.37)$$

It is useful to adopt a “comoving-observer gauge”, i.e., a gauge in which the time coordinate is the proper time on worldlines where  $dx^i = 0$ ,  $i = 1, 2, 3$  and such that

$g_{00} = a = 1$  or, equivalently,  $D_t = \partial_t$ . Furthermore, because of the homogeneity assumption, we can decompose  $R = R(\mu, t)$  as  $R = F(t)\tilde{R}(\mu)$ , so that

$$\dot{R} := \partial_t R = u = \dot{F}\tilde{R} = \frac{\dot{F}}{F}R. \quad (1.38)$$

The Einstein Eq. (1.35) becomes

$$\Gamma^2 = 1 + u^2 - \frac{2m}{R} = 1 + R^2 \left[ \left( \frac{\dot{F}}{F} \right)^2 - \frac{8\pi e}{3} \right] = 1 - \kappa \frac{R^2(\mu, t)}{S^2(t)}, \quad (1.39)$$

where  $\kappa = 0, \pm 1$  accounts for the sign of the term in square brackets and  $S$ , a function of time only, is just a shorthand for what is contained in the square brackets. Because of the decomposition of  $R$ , the ratio  $\tilde{R}/S$  is a function of  $r$  only and thus we can simply write

$$\Gamma^2 = 1 - \kappa r^2, \quad (1.40)$$

so that the line element (1.23) becomes

$$ds^2 = -a^2 dt^2 + b^2 dr^2 + R^2 d\Omega^2 = -dt^2 + S^2(t) \left[ \frac{dr^2}{1 - \kappa r^2} + r^2 d\Omega^2 \right]. \quad (1.41)$$

It is not difficult to recognize that the line element (1.41) is the metric of a Friedmann-Robertson-Walker cosmological solution, where the function  $S$  (i.e., the conformal factor of the spatial part of the metric) is simply the ‘‘scale factor’’. Similarly, it will not be surprising that, when expressed in this metric, the hydrodynamic and Einstein equations will essentially reduce to the Friedmann equations

$$\ddot{S} = -\frac{4\pi}{3}(e + p)S, \quad (1.42)$$

$$\dot{S}^2 - \frac{8\pi}{3}eS^2 = -\kappa. \quad (1.43)$$

Stated differently, the spatial part of the line element (1.41) describes geometries with different constant curvatures (i.e the curvature is the same everywhere but it is not constant in time), with the different geometries being selected by the values of the coefficient  $\kappa$ . In other words, in spherical symmetry, the dynamical spacetime of a collapsing (expanding) region occupied by homogeneous matter is a Friedmann-Robertson-Walker (FRW)-universe.

In cosmological terms, there are three possible solutions according to the value of  $\kappa$  and thus on the constant curvature ( $\kappa = -1$ , curved open universe;  $\kappa = 0$ : flat universe,  $\kappa = 1$ ; curved closed universe). Clearly, the relevant solution in the context of an OS collapse is the one with positive constant curvature (i.e.,  $\kappa = 1$ ) in

which case the line element can be expressed in terms of comoving hyperspherical coordinates  $(\chi, \theta, \phi)$

$$ds^2 = -d\tau^2 + S(\tau)[d\chi^2 + \sin^2 \chi d\Omega^2], \quad (1.44)$$

where  $\chi = \sin^{-1} r$ .

There is an important difference between the FRW universe and the spacetime of an OS collapse, since in the latter case not all of the spacetime is occupied by matter (the dust sphere has initially a finite radial size  $R_0$ ) and the vacuum region corresponding to  $R > R_0$  is described by a Schwarzschild spacetime. The matching between the two regions can be done at the surface of the star by requiring the continuity of the metric via, say, the continuity of the proper circumference

$$\mathcal{C}_{\text{Schw.}} := \int \sqrt{g_{\phi\phi}} d\phi = 2\pi R_0 = \mathcal{C}_{\text{FRW}} := 2\pi S \sin \chi_0. \quad (1.45)$$

Since (1.45) must hold at all times, we have that

$$R_0 = S \sin \chi_0. \quad (1.46)$$

Let us now consider the equations of motion in the collapsing region of the spacetime. In this case, Eq. (1.34), reduces to  $D_t m = 0$ , thus implying that  $m$  is not a function of time but of radius only, i.e.,  $m = m(\mu)$  as it should be in the absence of shocks. Similarly, Eq. (1.32) reduces to

$$D_t u = -m/R^2, \quad (1.47)$$

which is essentially the geodetic equation. The trajectory of any shell can therefore be obtained through a time integration of (1.47) and is given by

$$\dot{R} := \frac{dR}{d\tau} = D_t R = \left( \frac{2m}{R} - \frac{2m}{R_0} \right)^{1/2}. \quad (1.48)$$

In other words, a shell of dust will go from  $R_0$  to  $R = 0$  in a finite proper time

$$\tau = \frac{\pi}{2} R_0 \left( \frac{R_0}{2M} \right)^{1/2}. \quad (1.49)$$

Note that this time will be the same for all initial radial positions  $R$ ; this is a trivial consequence of the uniformity in density, for which the ratio  $R^3/m(R)$  is constant.

Once expressed in the coordinate system (1.44) and after introducing the ‘‘cycloid parameter’’  $\eta \in [0, \pi]$  defined by  $d\eta = d\tau/S$ , the equations of motion take the

simpler form

$$R = \frac{R_0}{2}(1 + \cos \eta), \quad S(\eta(\tau)) = \frac{S_m}{2}(1 + \cos \eta), \quad \tau = \frac{S_m}{2}(\eta + \sin \eta), \quad (1.50)$$

where  $\eta$  is playing the role of a time coordinate ( $\eta = 0$  at the beginning of collapse and  $\eta = \pi$  at the end).

Using now Eq. (1.50) and the condition (1.45), we find that

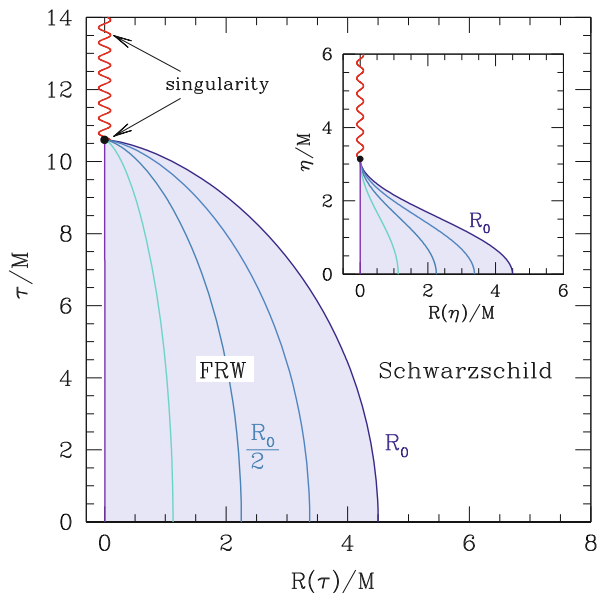
$$S_m = \left( \frac{R_0^3}{2M} \right)^{1/2}, \quad \chi_0 = \sin^{-1} \left( \frac{2M}{R_0} \right)^{1/2}. \quad (1.51)$$

It is particularly interesting to calculate the proper time  $\tau$  at which a shell initially at  $R_0$  reaches  $R = 2M$ . This can be computed from (1.50) and is given by

$$\tau_{2M} = \left( \frac{R_0^3}{2M} \right)^{1/2} (\eta_{2M} + \sin \eta_{2M}), \quad (1.52)$$

where  $\eta_{2M} := \cos^{-1}(4M/R_0 - 1)$ . These expressions will be useful in the following section to discuss what happens to outgoing photons as the collapse proceeds. The dynamics of OS collapse is summarised in Fig. 1.1.

**Fig. 1.1** Schematic diagram showing the worldlines of different collapsing radial shells in a  $(R, \tau)$  spacetime diagram. The various lines refer to shells initially at  $0$ ,  $(1/4)R_0$ ,  $(1/2)R_0$ ,  $(3/4)R_0$ , and  $R_0$ , and the lavender shaded area represents the stellar interior. Note that they all reach the singularity at the same proper time  $\tau = \frac{\pi}{2} \left( \frac{R_0^3}{2M} \right)^{1/2}$ . Also reported in the inset are the same worldlines but shown as a function of the cycloid parameter  $\eta$  [figure taken from [1]]



## 1.4 OS Collapse: Trapped Surfaces

Assuming the cosmic censorship to hold, namely, that the physical singularity is always hidden behind by a null surface that photons cannot leave, i.e., the *event horizon*, the final result of the spherical collapse is a Schwarzschild black hole. However, the Schwarzschild solution will be reached only asymptotically and is interesting to ask how the event horizon is formed during the collapse. In practice we need to study the trajectory of the outermost outgoing photon that was not able to reach null infinity. Similarly, we can calculate where, at each instant during the collapse, the last outgoing photon will be sent and reach null infinity. This surface will mark the outermost trapped surface, i.e., the *apparent horizon* and by definition it will always be contained within the event horizon.

Let us consider therefore the worldline of an *radially outgoing photon*. In this case,  $ds^2 = 0 = d\theta = d\phi$  and the line element (1.44) then yields the curves

$$\frac{d\chi}{d\tau} = \pm \frac{1}{S(\tau)}, \quad (1.53)$$

Using now the cycloid parameter  $\eta$  [cf. Eq. (1.50)], it is easy to show that these photons propagate along straight lines in a  $(\chi, \eta)$  plane

$$\frac{d\chi}{d\eta} = \pm 1, \quad (1.54)$$

i.e., they follow curves of the type

$$\chi = \chi_e \pm (\eta - \eta_e), \quad (1.55)$$

where  $\chi_e$  and  $\eta_e$  are the “place” and “time” of emission, respectively. A swarm of outgoing photons will be *trapped* if their proper area will not grow in time, i.e., if

$$\frac{d\mathcal{A}}{d\eta} \leq 0, \quad (1.56)$$

where  $\mathcal{A} := \int \sqrt{g_{\theta\theta}g_{\phi\phi}}d\theta d\phi$ . Writing out the condition (1.56) explicitly yields

$$\eta_e \geq \pi - 2\chi_e, \quad (1.57)$$

which indicates that any outgoing photon emitted at a position  $\chi_e$  and at a time  $\eta_e$  will be able to propagate out if and only if  $\eta_e$  is smaller than  $\pi - 2\chi_e$ . In practice, this condition singles out a region in a  $(\chi, \eta)$  plane, which trapped photons cannot leave.

Among all the possible trapped surfaces, the most important is certainly the outermost one since it will discriminate between the photons that will propagate to null infinity from the ones that will be trapped. Such a surface selects the apparent

horizon and since  $\chi_e \leq \chi_0$  (the emission takes place within the star) it is simply expressed as

$$\eta_{\text{ah}} = \pi - 2\chi_0 = 2 \cos^{-1} \left( \frac{2M}{R_0} \right)^{1/2}, \quad (1.58)$$

where we have used expression (1.51) to derive the last term in (1.58).

A natural question to ask this point is: when does the apparent horizon first form and where is it located? Luckily, answering these questions in the case of an OS collapse is particularly simple and reveals that the *apparent horizons first forms when the stellar surface crosses  $R = 2M$* . Note that this is true only in the OS collapse.

Finally, we consider the evolution of the event horizon which is defined as the surface for which the equality in condition (1.56) holds. Using the constraint that the event horizon is always outside or coincides with the apparent horizon, we can set  $\chi_{\text{eh}} = \chi_{\text{ah}}$  when  $\eta = \eta_{\text{ah}}$ , so that the worldline for the event horizon is given by

$$\chi_{\text{eh}} = \chi_0 + (\eta - \eta_{\text{ah}}), \quad (1.59)$$

for  $\eta \leq \eta_{\text{ah}}$ . Using now the circumferential radial coordinate we can write that

$$R_{\text{eh}} = \frac{1}{2} \left( \frac{R_0^3}{2M} \right)^{1/2} (1 + \cos \eta) \sin(\chi_0 + \eta - \eta_{\text{ah}}). \quad (1.60)$$

An important property to be deduced from (1.60) is that the event horizon starts from a zero radius and then progressively grows to reach  $R = 2M$ ; this is to be contrasted with what happens for the apparent horizon, that is first formed with a nonzero radial size.

The dynamics of the trapped surfaces is summarised in Fig. 1.2, which is similar to Fig. 1.1, but where we have reported the worldline of the stellar surface  $R_0(\tau)$  (dark blue line), that of the event horizon (green dashed line) and of the apparent horizon (orange solid line). Note that the event horizon grows from zero size and reaches the value  $2M$  when the stellar surface is at that position. This also marks the time when the inward-expanding apparent horizon is formed, which then shrinks to zero size as the dust star approaches the “covered” singularity. Note also that another outward expanding apparent horizon is formed at  $\tau_{2M}$ , but this then coincides with the event horizon. The trapped regions inside the event horizon and outside the shrinking apparent horizon are marked with a light-green and with an orange shaded area, respectively. Much of what we have learnt about the dynamics of trapped surfaces in the OS collapse continues to hold true also in the case of the collapse of a perfect fluid, where however the apparent horizon is also formed earlier because of the additional contribution of the fluid compression.

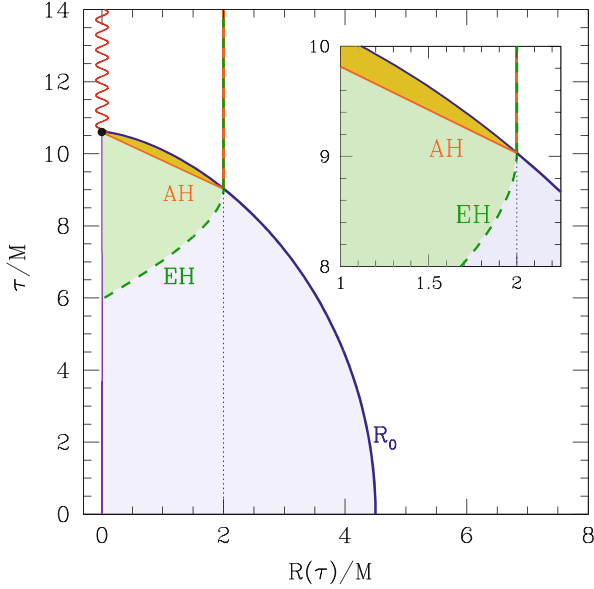


**Fig. 1.2** Schematic diagram showing the worldlines of the event horizon (EH), of the apparent horizon (AH) and of the stellar surface ( $R_0$ ). The inset offers a magnified view, where it is possible to note that the event and apparent horizons coincide after the stellar surface has reached  $R = 2M$  [figure taken from [1]]

The two panels of Fig. 1.3 offer instead a summary of the dynamics of the most relevant surfaces during the collapse of uniformly rotating fluid stars [7–11]. First, in the case of a slowly rotating star, i.e., model D1 on the left panel, the differences between the equatorial and polar circumferential radii of the two trapped surfaces are very small and emerge only in the inset which offers a magnified view of the worldlines during the final stages of the collapse. This is not the case for a rapidly rotating star, i.e., model D4 on the right panel, for which the differences are much more evident and can be appreciated also in the main panel. Second, the worldlines of the stellar surface are very different in the two cases. In particular, for the slowly rotating model, the star collapses smoothly and the worldline always has a negative slope, thus reaching progressively smaller radii as the evolution proceeds. By time  $t \simeq 0.59$  ms, the stellar equatorial circumferential radius has shrunk below the corresponding value of the event horizon. In the case of the rapidly rotating model D4, on the other hand, this is no longer true and after an initial phase which is similar to the one described for D1, the worldline does not reach smaller radii. Rather, the stellar surface slows its inward motion and at around  $t \sim 0.6$  ms the stellar equatorial circumferential radius does not vary appreciably. Indeed, the right panel of Fig. 1.3 shows that at this stage the stellar surface moves to slightly larger radii. This behaviour marks the phase in which a flattened configuration has been produced and the material at the outer edge of the disc experiences a stall. As

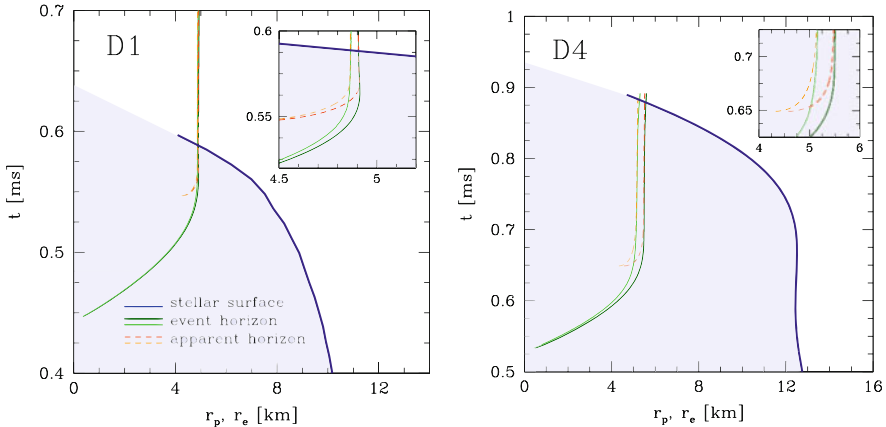


**Fig. 1.3** Evolution of the most relevant surfaces during the collapse for the cases of slowly and rapidly rotating stars. *Solid, dashed and dotted lines* represent the worldlines of the circumferential radii of the event horizon, of the apparent horizon and of the stellar surface, respectively. Note that for the horizons we plot both the equatorial and the polar circumferential radii, while only the equatorial circumferential radius is shown for the stellar surface. Shown in the insets are the magnified views of the worldlines during the final stages of the collapse [figure taken from [1]]

the collapse proceeds, however, also this material will not be able to sustain its orbital motion and after  $t \sim 0.7$  ms the worldline moves to smaller radii again. By a time  $t \simeq 0.9$  ms, the stellar equatorial circumferential radius has shrunk below the corresponding value of the event horizon.

## 1.5 Geodesic Motion in Schwarzschild and Kerr Spacetimes

Now that we have discussed that a fluid configuration can reach situations in which an equilibrium is no longer possible and have investigated what happens when such a configuration collapses to a black hole, we can move on and study geodesic motion in black-hole spacetimes. Indeed, the study of “test-particle” motion in a given spacetime geometry is very important since it allows one to highlight some of the properties of the spacetime under investigation without having to resort to the full system of Einstein equations. The particle needs to be a “test” particle (small enough not to perturb the spacetime), neutral (not to react to electromagnetic forces) spherical (so as not to be subject to torques), etc. From a pictorial point of view, the study of the motion of test-particles is not very different from “probing” the properties of a hole by throwing stones into it.

Test-particles move along “geodesics”. There are at least two different and equivalent definitions of geodesics. According to the first definition, a geodesic in affine geometry is a curve  $x^\mu = x^\mu(\lambda)$  that parallel transports its tangent vector  $u^\alpha = dx^\alpha/d\lambda$ . I recall that a four-vector  $\mathbf{v}$  is parallel transported along a curve  $x(\lambda)$

with tangent  $\mathbf{u}$  if  $\nabla_{\mathbf{u}}\mathbf{v} = 0$ . In component form this is equivalent to

$$u^\beta \nabla_\beta v^\alpha = u^\beta (\partial_\beta v^\alpha + \Gamma_{\beta\mu}^\alpha v^\mu) = 0, \quad (1.61)$$

where we introduced the covariant derivative. Hence, a geodesic curve should be seen as the solution nonlinear system of equations

$$\frac{d^2 x^\alpha}{d\lambda^2} + \Gamma_{\beta\mu}^\alpha \frac{dx^\beta}{d\lambda} \frac{dx^\mu}{d\lambda}. \quad (1.62)$$

In the (pseudo)-Riemannian case the coefficients of the affine connection are the Christoffel symbols

$$\Gamma_{\beta\mu}^\alpha = \frac{1}{2} g^{\alpha\sigma} (\partial_\mu g_{\sigma\beta} + \partial_\beta g_{\sigma\mu} - \partial_\sigma g_{\beta\mu}). \quad (1.63)$$

In flat space  $\Gamma_{\beta\mu}^\alpha = 0$  and the geodesics are straight lines. This is why it is commonly stated that geodesics are the analogues of straight lines in curved space. This idea is strengthened by the second possible definition of geodesics as the curves joining two given events  $A$  and  $B$  that are of extremal length. Here one derives the geodesic equations from a variational principle

$$\delta \int_A^B ds = 0, \quad (1.64)$$

where

$$ds^2 = g_{\alpha\beta} dx^\alpha dx^\beta, \quad (1.65)$$

is the spacetime interval between  $A$  and  $B$  [2–4]. The above variational problem can be shown to be equivalent to the following one

$$\delta \int_{\lambda_1}^{\lambda_2} \frac{1}{2} g_{\alpha\beta}(x) \dot{x}^\alpha \dot{x}^\beta d\lambda = 0, \quad (1.66)$$

where  $\lambda$  is an affine parameter along the curve and the overdot indicates derivative with respect to this parameter. The geodesic equations (1.62) then coincide with the corresponding Euler-Lagrange equations

$$\frac{d}{d\lambda} \frac{\partial L}{\partial \dot{x}^\alpha} = \frac{\partial L}{\partial x^\alpha}, \quad (1.67)$$

where the Lagrangian is given by

$$L = \frac{1}{2} g_{\alpha\beta}(x) \dot{x}^\alpha \dot{x}^\beta, \quad (1.68)$$

and the momenta conjugate to the coordinates  $x^\alpha$  are introduced in the usual way

$$p_\alpha = \frac{\partial L}{\partial \dot{x}^\alpha}, \quad (1.69)$$

Obviously the momentum  $p_\alpha$  is conserved when the metric does not depend on the coordinate  $x^\alpha$ .

For a Schwarzschild black hole in Schwarzschild coordinates, the metric reads

$$ds^2 = -\left(1 - \frac{2M}{r}\right) dt^2 + \left(1 - \frac{2M}{r}\right)^{-1} dr^2 + r^2 (d\theta^2 + \sin^2 \theta d\phi^2), \quad (1.70)$$

and the Lagrangian describing geodesic motion of is given by

$$2L = -\left(1 - \frac{2M}{r}\right) \dot{t}^2 + \left(1 - \frac{2M}{r}\right)^{-1} \dot{r}^2 + r^2 (\dot{\theta}^2 + \sin^2 \theta \dot{\phi}^2). \quad (1.71)$$

Because the metric does not depend on  $t$  and  $\phi$ , the corresponding Euler-Lagrange equations express conservation laws of the conjugate momenta

$$-p_t = \left(1 - \frac{2M}{r}\right) \dot{t} = E, \quad (1.72)$$

$$\frac{d}{d\lambda} p_t = 0, \quad (1.73)$$

$$p_\phi = r^2 \sin^2 \theta \dot{\phi} = l, \quad (1.74)$$

$$\frac{d}{d\lambda} p_\phi = 0, \quad (1.75)$$

where  $\lambda = \tau/m_0$ , and with  $\tau$  being the proper time of a massive particle of rest mass  $m_0$ . Note that the equation corresponding to the  $\theta$  coordinate

$$\frac{d}{d\lambda} r^2 \dot{\theta} = r^2 \sin \theta \cos \theta \dot{\phi}^2, \quad (1.76)$$

is simply stating that the orbit is planar and hereafter I will take  $\theta = \pi/2$  without loss of generality.

In order to appreciate the physical meaning of the constants  $E$  and  $l$  it is useful to consider how they are related to measurements made by locally static observers. To this end we introduce an orthonormal tetrad such that

$$\mathbf{e}_{\hat{\alpha}} \cdot \mathbf{e}_{\hat{\beta}} = \eta_{\hat{\alpha}\hat{\beta}}, \quad \tilde{\omega}^{\hat{\alpha}} \cdot \tilde{\omega}^{\hat{\beta}} = \eta^{\hat{\alpha}\hat{\beta}}, \quad (1.77)$$

where  $\tilde{\omega}$ s are the corresponding one-forms and  $\eta_{\hat{\alpha}\hat{\beta}} = \text{diag}(-1, 1, 1, 1)$  is the flat Minkowski metric. Requiring orthonormality and stationarity, one easily obtains

that

$$\mathbf{e}_{\hat{t}} = \left(1 - \frac{2M}{r}\right)^{-\frac{1}{2}} \mathbf{e}_t, \quad \tilde{\omega}^{\hat{t}} = \left(1 - \frac{2M}{r}\right)^{\frac{1}{2}} \tilde{\omega}^t, \quad (1.78)$$

$$\mathbf{e}_{\hat{r}} = \left(1 - \frac{2M}{r}\right)^{\frac{1}{2}} \mathbf{e}_r, \quad \tilde{\omega}^{\hat{r}} = \left(1 - \frac{2M}{r}\right)^{-\frac{1}{2}} \tilde{\omega}^r, \quad (1.79)$$

$$\mathbf{e}_{\hat{\theta}} = \frac{1}{r} \mathbf{e}_\theta, \quad \tilde{\omega}^{\hat{\theta}} = r \tilde{\omega}^\theta, \quad (1.80)$$

$$\mathbf{e}_{\hat{\phi}} = \frac{1}{r \sin \theta} \mathbf{e}_\phi, \quad \tilde{\omega}^{\hat{\phi}} = r \sin \theta \tilde{\omega}^\theta, \quad (1.81)$$

$$(1.82)$$

where  $\mathbf{e}_\alpha^\beta = \delta_\alpha^\beta$ . In special relativity, the invariant mass  $\mathbf{p} \cdot \mathbf{p} = p^2 = -m^2$ , coincides with the rest mass measured by a static observer

$$\mathbf{p} \cdot \mathbf{u} = p_0 u^0 = -p_0 = -m. \quad (1.83)$$

The above identity may be rewritten as follows

$$E = -p_\alpha u^\alpha = -p_\alpha e_t^\alpha = -p_t = -\eta_{tt} p^t = p^t. \quad (1.84)$$

In a Schwarzschild spacetime

$$E_{loc} = -p_\alpha e_{\hat{t}}^\alpha = -p_\alpha e_t^\alpha \left(1 - \frac{2M}{r}\right)^{-\frac{1}{2}} = E \left(1 - \frac{2M}{r}\right)^{-\frac{1}{2}} > E, \quad (1.85)$$

and the two energies are related by the redshift formula

$$\frac{E_\infty}{E_{loc}} = \frac{\nu_\infty}{\nu_{loc}} = \left(1 - \frac{2M}{r}\right)^{\frac{1}{2}}, \quad (1.86)$$

where  $\nu_\infty$  and  $\nu_{loc}$  are, for instance, the frequencies of a photon as measured at spatial infinity and near the black hole, respectively.

Similarly, we can define the angular velocity measured by a locally static observer

$$v^{\hat{\phi}} = \frac{p_\alpha e_{\hat{\phi}}^\alpha}{p_\alpha e_{\hat{t}}^\alpha} = \frac{l}{r \sin \theta E_{loc}} \quad (1.87)$$

so that the constant of motion

$$l = v^{\hat{\phi}} r \sin \theta E_{loc}, \quad (1.88)$$

can be seen as the conserved relativistic angular momentum.

### 1.5.1 Massive Particles

Hereafter, I will distinguish the motion of massive and massless particles, concentrating first on the former and leaving the latter to Sect. 1.5.2. In this case, the Lagrangian is normalised by the mass by the relation  $2L = -m_0^2$ . In this way, Eq. (1.71) becomes

$$\frac{dr}{d\tau} = \pm \left[ \tilde{E}^2 - \left(1 - \frac{2M}{r}\right) \left(1 + \frac{\tilde{l}^2}{r^2}\right) \right]^{\frac{1}{2}}, \quad (1.89)$$

where  $\tilde{l} := l/m_0$  and  $\tilde{E} := E/m_0$ . When  $\tilde{l} = 0$  and  $\tilde{E} = (1 - 2M/R) < 1$ , Eq. (1.89) can be integrated to give

$$\tau = \sqrt{\frac{R^3}{8M}} \left( 2\sqrt{\frac{r}{R} - \frac{r^2}{R^2}} + \cos^{-1} \left( \frac{2r}{R} - 1 \right) \right), \quad (1.90)$$

so that  $\tau = 0$  when  $r = R$ . The remarkable fact is that the *proper* time to reach first the horizon, i.e.,  $r = 2M$  from any  $R > 2M$ , and then the singularity at  $r = 0$  is finite. To see this, one may introduce the cycloid parameter  $\eta$  as

$$r = \frac{R}{2}(1 + \cos \eta). \quad (1.91)$$

Equation (1.90) then becomes

$$\tau = \sqrt{\frac{R^3}{8M}} (\eta + \sin \eta), \quad (1.92)$$

which obviously coincides with the result found in Eq. (1.52) for the OS collapse: in both cases the motion is a free fall.

The situation is completely different when one integrates the equations of motion in terms of the coordinate time  $t$ . In this case, in fact, one gets

$$\frac{t}{2M} = \log \left| \frac{\sqrt{R/2M - 1} + \tan \eta/2}{\sqrt{R/2M - 1} - \tan \eta/2} \right| + \sqrt{\frac{R}{2M} - 1} \left[ \eta + \frac{R}{2M} (\eta + \sin \eta) \right]. \quad (1.93)$$

When  $r = 2M$  one has  $\tan \eta/2 = \sqrt{R/2M - 1}$ , so that it takes an infinite *coordinate* time to reach the horizon from any  $R > 2M$ . This behaviour reflects the singular properties of the event horizon and, at the same time, the fact that the singularity comes from the coordinates and it is not physical. This is seen, for instance, by calculating the curvature invariants, which are perfectly regular at the horizon and only diverge at  $r = 0$ .

The velocity measured by a static observer is

$$\begin{aligned} v^{\hat{r}} &= \frac{p^{\hat{r}}}{p^{\hat{t}}} = \frac{p_{\hat{r}}}{p^{\hat{t}}} = \frac{p_{\alpha} e_{\hat{r}}^{\alpha}}{E_{loc}} = \frac{p_r \left(1 - \frac{2M}{r}\right)^{\frac{1}{2}}}{E_{loc}} = \frac{p^r}{E} = \frac{m}{E} \frac{dr}{d\tau} = \\ &= \frac{1}{\tilde{E}} \sqrt{\tilde{E}^2 - \left(1 - \frac{2M}{r}\right) \left(1 + \frac{\tilde{l}^2}{r^2}\right)}. \end{aligned} \quad (1.94)$$

Note that  $v^{\hat{r}} \rightarrow 1$  on the horizon irrespective of the values of  $\tilde{E}$  and  $\tilde{l}$ . In other words, a particle will cross the horizon at the speed of light independently of the initial conditions. In the case of radial fall from rest at infinity, i.e.,  $\tilde{E} = 1$  and  $\tilde{l} = 0$ , the above formula reproduces the Newtonian result

$$v^{\hat{r}} = \sqrt{\frac{2M}{r}}. \quad (1.95)$$

Let us consider now more general non-radial orbits and rewrite Eq. (1.89) as

$$\frac{dr}{d\tau} = \pm \left(\tilde{E}^2 - V(r, \tilde{l})\right)^{\frac{1}{2}}, \quad (1.96)$$

where

$$V := \left(1 - \frac{2M}{r}\right) \left(1 + \frac{\tilde{l}^2}{r^2}\right), \quad (1.97)$$

is the effective potential, which reduces to the Newtonian effective potential at large distances, namely (see Fig. 1.4)

$$V(r) \approx \left(1 - \frac{M}{r}\right) \left(1 + \frac{\tilde{l}^2}{2r^2}\right) = 1 - \frac{M}{r} + \frac{\tilde{l}^2}{2r^2} + \mathcal{O}\left(\frac{1}{r^3}\right) := V_{\text{Newt}}. \quad (1.98)$$

The radial equation (1.96) is also useful to classify the different types of orbits which are possible and which will essentially depend on the number of maxima and minima the effective potential will have for a given value of the specific angular momentum (if  $\tilde{l} = 0$  the orbit is simply radial and will connect any radial point with the origin). Let us assume, for the time being, that the specific angular momentum is such that it yields an effective potential with a local maximum with  $V > 1$ , and local minimum, just as illustrated in the left panel of Fig. 1.4, which refers to  $\tilde{l}/M = 4.1$ . In this case, using the specific energy  $\tilde{E}$  as a decreasing parameter, the

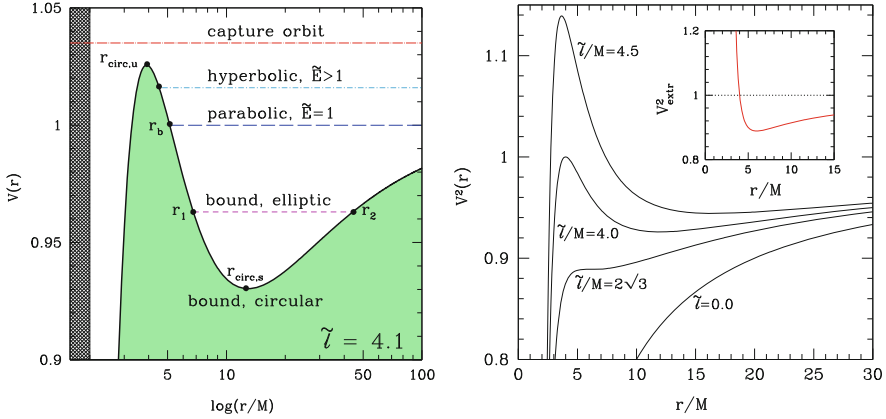


**Fig. 1.4** *Left panel:* effective potential  $V(r)$  for a value  $\tilde{l}/M = 4.1$  of the specific angular momentum. Shown are the different types of orbits allowed: capture, marginally bound, marginally stable, *elliptic* and *circular*, as determined by the different values of the energy above the *green dashed area*. Shown as *black shading* is the region inside the horizon, with the radial scale set to be logarithmic. *Right panel:* effective potential  $V(r)$  of the Schwarzschild metric for some values of the angular momentum  $\tilde{l}$ . The *inset* shows the value of the effective potential at the local extrema and it should be noted that the radial scale is linear

orbits can be:

- *capture orbit:* no intersection is possible between the effective potential and a constant-energy level. No matter how large the angular momentum, there is always a value of the energy that makes the particle reach the origin. This is to be contrasted with the Newtonian case, where the effective potential diverges as  $r \rightarrow 0$ , and thus no matter how small (but nonzero) the angular momentum, a particle in a Newtonian orbit will never reach the origin (i.e., the Newtonian potential has a zero *capture cross-section*).
- *circular, unstable orbit:* this is located at the local maximum of the effective potential,  $r_{\text{circ,u}}$ , where  $dr/d\tau = 0$ , and is such that any perturbation will move the particle either to smaller or to larger radii.
- *hyperbolic, unbound orbits:* these correspond to orbits of particles with energies at spatial infinity larger than one (i.e., with positive velocity), that move towards the origin till reaching a minimum radial position at which  $dr/d\tau = 0$ , i.e., a *turning point*, from where they return to infinity.
- *parabolic, bound orbit:* this corresponds to an orbit of a particle with energy at spatial infinity equal to one (i.e., at rest), that moves towards the origin till reaching a *turning point*,  $r_b$ . For  $\tilde{l}/M = 4$ , the turning point coincides with the unstable circular orbit  $r_{\text{circ,u}}$  and is located at  $4M$  (see below).

- “*elliptic*”, *bound orbits*: these correspond to orbits with energies at spatial infinity less than one (i.e., bound particles) that have two turning points at  $r_1$  and  $r_2$ .<sup>2</sup>
- *circular, stable orbit*: this is located at the local minimum of the effective potential,  $r_{\text{circ},s}$ , where  $dr/d\tau = 0$ , and is such that any small perturbation away from the stable orbit will move the particle back to it.

The values of the specific angular momentum for which the effective potential shows both local minima and maxima, i.e., for which  $\partial_r V(r) = 0$ , and thus for which circular orbits exist, is given by

$$\tilde{l}^2 = \frac{Mr^2}{r - 3M}, \quad (1.99)$$

with corresponding energies

$$\tilde{E}^2 = \frac{(r - 2M)^2}{r(r - 3M)}. \quad (1.100)$$

To ensure that the right-hand side is positive, such extremal points exist only for  $\tilde{l}/M \geq 2\sqrt{3}$ . Furthermore, for  $\tilde{l}_{\text{ms}}/M = 2\sqrt{3} \simeq 3.46$ , the stable and unstable circular orbits coincide, leading to an *inflection point* at the radius  $r_{\text{ms}} = 6M$ , which is also called the *marginally stable* radius. The corresponding orbit is also known as the *innermost stable circular orbit* or *ISCO* and because this represents the smallest possible radius for a stable circular orbit, it is often taken to mark the inner edge of an accretion disc around a black hole.

The variation of the effective potential with the specific angular momentum is illustrated in the right panel of Fig. 1.4, while the inset shows the values of the effective potential at the local extrema (which coincide with the energies of the unstable circular orbits), and is given by

$$V_{\text{extr}}^2(r) = \frac{4M^2 (r/2M - 1)^2}{r(r - 3M)}. \quad (1.101)$$

Setting  $V_{\text{extr}}(r) = 1$  will mark the position of the *marginally bound orbit*  $r_{\text{mb}} = 4M$ , namely, the smallest radius for a bound, circular but unstable orbit. A particle leaving spatial infinity at rest (i.e., with  $\tilde{E} = 1$ ), will move on a parabolic orbit down to  $r = r_{\text{mb}}$ , where it can remain on a circular orbit but in unstable equilibrium.

In summary, unstable circular orbits exist for

$$3M = r_{\text{ph}} \leq r < r_{\text{ms}} = 6M, \quad \iff \quad 2\sqrt{3} \leq \tilde{l}/M < \infty, \quad (1.102)$$

---

<sup>2</sup>Note that these orbits are not closed because of the advance of the periastron, another general-relativistic effect of the motion in a gravitational field [2]. Hence, the defining property of these orbits is that of having two turning points and not that of being closed ellipses.

while stable circular orbits exist for

$$6M = r_{\text{ms}} \leq r < \infty, \quad \iff \quad 2\sqrt{3} \leq \tilde{l}/M < \infty. \quad (1.103)$$

Using Eq.(1.101), it is not difficult to estimate that the energy corresponding to the ISCO is  $\tilde{E}_{\text{ms}} = \sqrt{8/9} \simeq 0.943$ , and this apparently simple result calls for an important comment. Consider, in fact, a particle progressively moving from a circular orbit to a neighbouring one and losing part of its energy in the transition (e.g., a fluid element in an accretion disc). The total energy that can be lost when inspiralling from spatial infinity down to the ISCO is  $\Delta E = (1 - \tilde{E}_{\text{ms}}) \simeq 0.057$ , implying an efficiency in the conversion of the binding energy of  $\simeq 6\%$ . When comparing this with the efficiency of nuclear fission (i.e.,  $\sim 0.1\%$ ) or of nuclear fusion (i.e.,  $\sim 0.4\%$ ), it becomes clear that accretion onto a black hole represents one of the most efficient processes to extract energy. As we will comment in the following section, this efficiency can be further increased in the case of a rotating black hole.

For a circular orbit it is also possible to compute the angular velocity as seen by an observer at infinity

$$\Omega = \frac{\dot{\phi}}{\dot{t}} = \frac{\tilde{l}^2}{r^2} \left( \frac{1 - 2M/r}{\tilde{E}} \right). \quad (1.104)$$

In the case of circular orbits, by using Eqs. (1.99) and (1.100) we get

$$\Omega = \sqrt{\frac{M}{r^3}}, \quad (1.105)$$

exactly as in Newtonian gravity. On the other hand

$$v^{\hat{\phi}} = \frac{l}{rE} \left( 1 - \frac{2M}{r} \right)^{\frac{1}{2}} \rightarrow 0 \quad \text{for } r \rightarrow 2M, \quad (1.106)$$

that is, all the particles, even those with angular momentum, enter the event horizon on radial trajectories.

Let us now calculate the cross section for a particle flying by the black hole where the maximum impact parameter is  $b_{\text{max}} = \lim_{r \rightarrow \infty} r \sin \phi$ . Since

$$\left( \frac{dr}{d\phi} \right)^2 = \left( \frac{\dot{r}}{\dot{\phi}} \right)^2 = \frac{r^4 [\tilde{E}^2 - (1 - 2M/r)(1 + \tilde{l}^2/r^2)]}{\tilde{l}^2}, \quad (1.107)$$

for  $r \rightarrow \infty$  and  $\phi \ll 1$  we then have

$$\left( \frac{dr}{r^2 d\phi} \right)^2 \simeq \frac{1}{b^2} \simeq \frac{\tilde{E}^2 - 1}{\tilde{l}^2} = \frac{v_{\infty}^2}{\tilde{l}^2 (1 - v_{\infty}^2)}, \quad (1.108)$$

or else

$$\tilde{l} = \frac{bv_\infty}{\sqrt{1-v_\infty^2}} \simeq bv_\infty. \quad (1.109)$$

If the particle is non-relativistic at infinity, then  $v_\infty \ll 1$ ,  $\tilde{E} \simeq 1$  and the capture occurs for  $\tilde{l} < 4M$  and therefore<sup>3</sup>  $b_{\max} = 4M/v_\infty$ ; in turn, this implies that

$$\sigma_{\text{capture}} = \pi b_{\max}^2 = \frac{16\pi M^2}{v_\infty^2}, \quad (1.110)$$

This result may be compared with the Newtonian result  $\sigma_{\text{Newt}} = 2\pi MR/v_\infty^2$  relative to a gravitating sphere of mass  $M$  and radius  $R$ ; the comparison then suggests that a black hole captures nonrelativistic particles as if it were a sphere of radius  $R = 8M$ .

## 1.5.2 Massless Particles

In the case of massless particles, the Lagrangian is normalised to zero and thus reads

$$2L = -\left(1 - \frac{2M}{r}\right) \dot{t}^2 + \left(1 - \frac{2M}{r}\right)^{-1} \dot{r}^2 + r^2 \left(\dot{\theta}^2 + \sin^2 \theta \dot{\phi}^2\right) = 0, \quad (1.111)$$

and the Euler-Lagrange equations relative to the coordinates  $t$  and  $\phi$  are conservation laws, with  $E = -p_t$  and  $l = p_\phi$

$$\dot{t} = \frac{E}{(1 - 2M/r)}, \quad \dot{\phi} = \frac{l}{r^2}. \quad (1.112)$$

The equation corresponding to the  $r$  coordinate comes from  $L = 0$ :

$$\dot{r}^2 = E^2 - \frac{l^2}{r^2} \left(1 - \frac{2M}{r}\right). \quad (1.113)$$

The equivalence principle implies that the photon trajectory is independent of its energy. This can be seen by introducing a new affine parameter  $\lambda' = l\lambda$  and the photon impact parameter  $b = l/E$ , so that the previous equations can be rewritten

$$\dot{t} = \frac{E}{b(1 - 2M/r)}, \quad (1.114)$$

---

<sup>3</sup>Note that  $4M < b_{\max} < \infty$  and that  $b_{\max} \rightarrow \infty$  when  $v_\infty^2 \rightarrow 0$ . All particles are accreted or deflected.

$$\dot{\phi} = \frac{1}{r^2}, \quad (1.115)$$

$$i^2 = \frac{1}{b^2} - \frac{1}{r^2} \left( 1 - \frac{2M}{r} \right) = \frac{1}{b^2} - V_{ph}(r). \quad (1.116)$$

The effective potential in this case has a maximum of  $1/(27M^2)$  at  $r = 3M$ , which corresponds to the critical impact parameter  $b_c = 3\sqrt{3}M$ , so that the capture cross section for a photon from infinity is

$$\sigma_{ph} = 27\pi M^2. \quad (1.117)$$

The orbit at  $r = r_{ph} = 3M$  is the only circular orbit for a photon of impact parameter  $b_c$  and is usually referred to as the “light ring”.

An interesting question is whether the direction of emission plays a role in the propagation of a photon in the vicinity of a black hole. Also in this case we need to use the measurements made by locally static observers. For such observers the photon will propagate to infinity if either if  $v^{\hat{r}} > 0$ , or if  $v^{\hat{r}} < 0$  and  $b > 3\sqrt{3}$  (a photon can be shot towards a black hole and yet escape), where  $v^{\hat{r}}$  is the local photon velocity in the  $r$  direction and  $v^{\hat{a}}v_{\hat{a}} = v^{\hat{r}}v_{\hat{r}} + v^{\hat{\phi}}v_{\hat{\phi}} = 1$ . Let  $\psi$  denote the angle between the direction of propagation and the radial direction, so that  $v_{\hat{r}} = \cos \psi$  and  $v^{\hat{\phi}} = \sin \psi$ . It then follows that an ingoing photon escapes to infinity if

$$v^{\hat{\phi}} = \sin \psi = \frac{b}{r} \left( 1 - \frac{2M}{r} \right)^{\frac{1}{2}} > \frac{3\sqrt{3}M}{r} \left( 1 - \frac{2M}{r} \right)^{\frac{1}{2}}. \quad (1.118)$$

Conversely, an outgoing photon emitted between  $r = 2M$  and  $r = 3M$  escapes to infinity if

$$\sin \psi < \frac{3\sqrt{3}M}{r} \left( 1 - \frac{2M}{r} \right)^{\frac{1}{2}}. \quad (1.119)$$

### 1.5.3 Kerr Black Holes

In 1963, that is, almost 50 years after Schwarzschild’s work, Kerr found a stationary solution to the Einstein equations in vacuum, which describes the spacetime of a black hole of total mass  $M$  and angular momentum  $J$  [12]. This solution, which is also known as the *Kerr black-hole* solution and was later proven to be unique, reduces to the Schwarzschild solution in the limit of zero angular momentum. Since it includes the contributions of rotation, the Kerr black hole is not spherically symmetric, but axisymmetric about the direction of the angular momentum vector

of the black hole; furthermore, it is no longer a static solution, but a stationary one.<sup>4</sup> Due to the ubiquitous presence of rotation in astrophysical systems, this solution is considered to be the most realistic for studying any physical process that takes place in the vicinity of a black hole. Unfortunately, no analogue exists for the Kerr solution, which is unique in vacuum, but whose exterior in non-vacuum spacetimes depends on the properties of the matter source, e.g., mass and angular momentum distribution in the case of a relativistic star.

The line element for a Kerr black hole of mass  $M$  and angular momentum  $S$  in Boyer-Lindquist coordinates is

$$ds^2 = - \left( 1 - \frac{2Mr}{\Sigma} \right) dt^2 - \frac{4Mr \sin^2 \theta}{\Sigma} dt d\phi + \frac{\Sigma}{\Delta} dr^2 + \Sigma d\theta^2 + \left( r^2 + a^2 + \frac{2a^2 Mr \sin^2 \theta}{\Sigma} \right) \sin^2 \theta d\phi^2, \quad (1.120)$$

where  $a := S/M$  is the angular momentum per unit mass of the black hole ( $a/M \in [-1, 1]$ ) and

$$\Delta := r^2 - 2Mr + a^2, \quad \Sigma^2 := r^2 + a^2 \cos^2 \theta, \quad (1.121)$$

Clearly, the metric (1.120) reduces to the Schwarzschild metric (1.70) when  $a = 0$ .

Unlike in the Schwarzschild solution, where the surfaces of infinite redshift and of the event horizon coincide, the Kerr solution has two surfaces of infinite redshift, again obtained by imposing  $g_{tt} = 0$ , and are given by the condition

$$r_{s,\pm} = M \pm \sqrt{M^2 - a^2 \cos^2 \theta}. \quad (1.122)$$

The event horizons, on the other hand, can be determined from the divergence of the metric function  $g_{rr}$  and thus from setting  $\Delta = 0$ , which then yields the two surfaces

$$r_{eh,\pm} = M \pm \sqrt{M^2 - a^2}, \quad (1.123)$$

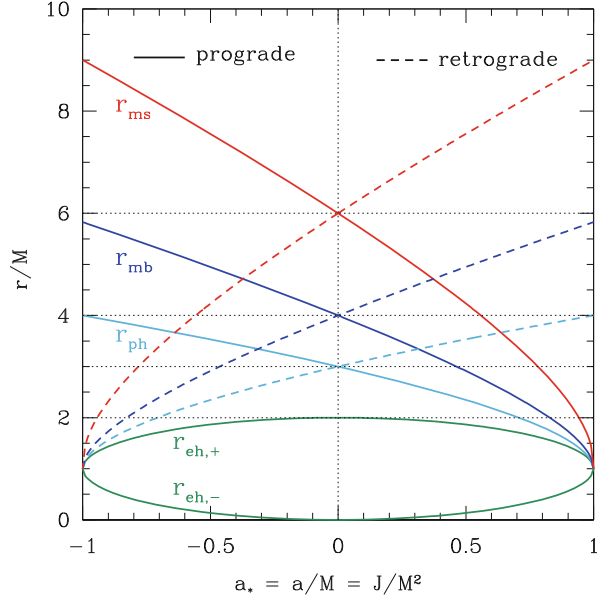
where the  $\pm$  sign denotes the outer (+) and inner (−) event horizon, respectively. Note that in the Schwarzschild limit  $r_{eh,-} = 0$ , and  $r_{eh,+} = 2M$ , as expected (see also Fig. 1.5).

The region between  $r_{s,+}$ , which is also called the *ergosphere*, and  $r_{eh,+}$  is also referred to as the *ergoregion*, since no static observers (i.e., observers seen as non-rotating from infinity) can exist and the whole spacetime is dragged into synchronous *corotation* by the black hole. This purely relativistic effect, which is also known as *frame dragging*, does not apply only to the ergoregion (where the

---

<sup>4</sup>The metric components are still independent of time but the solutions are affected by a time reversal, i.e., by a coordinate transformation  $t \rightarrow -t$ .

**Fig. 1.5** Relevant radii for equatorial orbits in a Kerr spacetime. Shown as a function of the dimensionless spin of the black hole,  $a/M$ , are respectively: the radii of the outer and inner event horizons  $r_{eh, \pm}$ , the radii of the marginally stable photon orbits  $r_{ph}$ , the radii of the marginally bound photon orbits  $r_{mb}$ , and the radii of the marginally stable orbits  $r_{ms}$ . *Continuous and dashed lines* help distinguish between prograde and retrograde orbits, respectively [figure taken from [1]]



corotation is unavoidable even for photons), but extends to the whole spacetime, although it becomes progressively weaker far from the black hole. As a result, an observer with zero angular momentum at infinity, or Zero Angular Momentum Observer (ZAMO), will not move radially towards the black hole, but will be set into rotation as seen from infinity. The importance of the ergosphere lies in that it can host physical processes that extract rotational energy from the black hole [2]. To see this, consider a particle with generic momenta

$$m \frac{dt}{d\tau} = p^t = g^{tt} p_t + g^{t\phi} p_\phi, \quad (1.124)$$

$$m \frac{d\phi}{d\tau} = p^\phi = g^{\phi t} p_t + g^{\phi\phi} p_\phi, \quad (1.125)$$

and thus with angular velocity

$$\Omega := \frac{d\phi}{dt} = \frac{p^\phi}{p^t}. \quad (1.126)$$

If the particle has zero angular momentum at spatial infinity, then  $p_\phi = 0$  and using the expression above it follows that

$$\Omega = \frac{g^{\phi t}}{g^{tt}} = \omega(r, t) = \frac{2Mra}{(r^2 + a^2)^2 - a^2 \Delta \sin^2 \theta}. \quad (1.127)$$

In other words, the particle will acquire an angular velocity (1.127) as it approaches the rotating black hole. The Lense-Thirring angular velocity  $\omega(r, t)$  is therefore the manifestation of the dragging of inertial frames and it decays as  $r^{-3}$ , thus more rapidly than the monopole component of the gravitational field.

As done for the Schwarzschild spacetime, it is possible to study the geodesic motion of test particles in the Kerr metric to gain insight into its properties. The particle motion in this case is far more complicated and, in addition to the energy and angular momentum,  $p_t = -E$  and  $p_\phi = l$ , a new constant of motion appears, i.e., the *Carter constant* [2]. Furthermore, the motion is planar only in the case of equatorial orbits, whose qualitative properties remain similar to the ones already encountered for a Schwarzschild spacetime. Hence, for simplicity I will concentrate here on the simplest cases of (planar) equatorial orbits (i.e., with  $\theta = \pi/2$ ) and considering mostly massive particles. The corresponding Lagrangian is then given by

$$2L = -\left(1 - \frac{2M}{r}\right)\dot{t}^2 - \frac{4aM}{r}\dot{t}\dot{\phi} + \frac{r^2}{\Delta}\dot{r}^2 + \left(r^2 + a^2 + \frac{2a^2M}{r}\right)\dot{\phi}^2 = -m_0^2, \quad (1.128)$$

so that the geodesic equations are

$$\dot{t} = \frac{1}{\Delta} \left[ \left( r^2 + a^2 + \frac{2a^2M}{r} \right) E - \frac{2Mal}{r} \right], \quad (1.129)$$

$$\dot{\phi} = \frac{1}{\Delta} \left[ \left( 1 - \frac{2M}{r} \right) l + \frac{2Ma}{r} E \right]. \quad (1.130)$$

Equation (1.128) is then rewritten as follows

$$r^3\dot{r}^2 = E^2(r^3 + 2Ma^2 + a^2r) - 4aMEl - l^2(r - 2M) - m^2r\Delta = \tilde{V}(E, l, r), \quad (1.131)$$

so that circular orbits correspond to energies and angular momenta

$$\tilde{E} = \frac{r^2 - 2Mr \pm a\sqrt{Mr}}{r(r^2 - 3Mr \pm 2a\sqrt{Mr})^{\frac{1}{2}}}, \quad (1.132)$$

$$\tilde{l} = \pm \frac{\sqrt{Mr}(r^2 \pm 2a\sqrt{Mr} + a^2)}{r(r^2 - 3Mr \pm 2a\sqrt{Mr})^{\frac{1}{2}}}, \quad (1.133)$$

where the plus sign correspond to co-rotating orbits and the minus to counter-rotating ones. Circular orbits then exist from infinity to the limit radius where the

energy diverges

$$r_{ph} = 2M \left( 1 + \cos \left( \frac{2}{3} \cos^{-1} \left( \pm \frac{a}{M} \right) \right) \right), \quad (1.134)$$

and these can even be at the horizon (i.e.,  $r_{ph} = M$ ) for corotating particles and a so-called “extremal” Kerr black hole (i.e., one with  $a = M$ ).

A marginally bound circular orbit is the orbit with the largest specific angular momentum and at rest at infinity. For  $r > r_{ph}$ , circular orbits are bound for

$$r > r_{mb} = 2M \mp a + 2\sqrt{M(M \mp a)}, \quad (1.135)$$

For each value of the black-hole spin  $a/M$ , stable circular orbits exist from spatial infinity down to the *marginally stable orbit*, or ISCO, given by

$$r_{ms,\pm} = r_{\text{ISCO}} = M \left[ 3 + Z_2 \mp \sqrt{(3 - Z_1)(3 + Z_1 + 2Z_2)} \right], \quad (1.136)$$

where

$$Z_1 := 1 + (1 - a^2)^{1/3} [(1 + a)^{1/3} + (1 - a)^{1/3}], \quad (1.137)$$

$$Z_2 := \sqrt{3a^2 + Z_1^2}. \quad (1.138)$$

Special values for the marginally stable radii  $r_{ms}$  are simple to compute and are given by (cf., Fig. 1.5)

$$r_{ms} = \begin{cases} 6M & \text{for } a/M = 0, \\ M & \text{for } a/M = 1, \\ 9M & \text{for } a/M = -1. \end{cases} \quad (1.139)$$

Figure 1.5 shows a useful summary of the relevant radii for equatorial orbits in a Kerr spacetime. Reported as a function of the dimensionless spin of the black hole,  $a/M$ , are respectively: the radii of the outer and inner event horizons  $r_{eh,\pm}$ , the radii of the marginally stable photon orbits  $r_{ph}$ , the radii of the marginally bound photon orbits  $r_{mb}$ , and the radii of the marginally stable orbits  $r_{ms}$ . Continuous and dashed lines help distinguish between prograde and retrograde orbits, respectively. Note that for  $a/M = 1$ , i.e., for an *extremal Kerr black hole*, a number of radii for prograde orbits tend to coincide, i.e.,  $r_{ms} = r_{ph} = r_{eh,+} = M$  (obviously, the same happens for retrograde orbits around black holes with  $a/M = -1$ ).

As a final remark, I note that Kerr black holes are also much more efficient in extracting energy. Indeed, since stable circular orbits exist down to the horizon, they can have there extremely small energies and as small as  $\tilde{E}_{ms} = 0.577$ . As a result, a particle accreting from spatial infinity down to the ISCO of an extremal Kerr black hole will have lost an amount of energy  $E = (1 - \tilde{E}_{ms}) = 0.43$ , implying

a conversion of  $\sim 43\%$  of the binding energy. This enormous efficiency explains why models of accretion discs onto Kerr black holes represent the best candidates to explain the vast amounts of energy radiated in active galactic nuclei (AGN).

## 1.6 Black Holes Produced from Binary Mergers

Despite the almost unnatural simplicity with which the problem can be formulated (black holes are after all the simplest macroscopical objects we know), the final evolution of a binary system of black holes is an impressively complex problem to solve. At the same time, this very simple process plays a fundamental role in astrophysics, in cosmology, in gravitational-wave astronomy, and of course in general relativity. Recent progress in numerical relativity initiated by the works in [13–15], have made it now possible to compute the different stages of the evolution, starting from the inspiral at large separations, for which post-Newtonian (PN) calculations provide an accurate description, through the highly relativistic merger, and finally to the ringdown.

As long as the two black holes are not extremal and have masses which are not too different from each other, no major technical obstacle now prevents the solution of this problem in full generality and with an overall error which can be brought down to less than 1% or less. Yet, obtaining such a solution still requires a formidable computational power sustained over several days. Even for the simplest set of initial data, namely those considering two black holes in quasi-circular orbits, the space of parameters is too vast to be explored entirely through numerical-relativity calculations. Furthermore, many studies of astrophysical interest, such as many-body simulations of galaxy mergers, or hierarchical models of black-hole formation, span a statistically large space of parameters and are only remotely interested in the evolution of the system during the last few tens of orbits and much more interested in determining the properties of the final black hole when the system is still widely separated.

In order to accommodate these two distinct and contrasting needs, namely that of sampling the largest possible space of parameters and that of reducing the computational costs, a number of analytical or semi-analytic approaches have been developed over the last couple of years. In most of these approaches the inspiral and merger is considered as a process that takes, as input, two black holes of initial masses  $M_1$ ,  $M_2$  and spin vectors  $\mathbf{S}_1$ ,  $\mathbf{S}_2$  and produces, as output, a third black hole of mass  $M_{\text{fin}}$ , spin  $\mathbf{S}_{\text{fin}}$  and recoil velocity  $\mathbf{v}_{\text{kick}}$ . Mathematically, therefore, one is searching for a mapping between the initial seven-dimensional space of parameters (i.e., the one containing the six spin components  $S_{1,2}^i$  and the mass ratio  $q := M_2/M_1$ ) to two a five-dimensional one, i.e., the one containing the three components of the final spin vector, the magnitude of the recoil velocity, and the mass of the final black hole. Clearly this is a degenerate mapping (two different initial configurations can lead to the same final one) and it would seem a formidable task to accomplish given the highly nonlinear features of the few last orbits. Yet, all

of these studies have shown that the final spin vector and the final recoil velocity vector, can be estimated to remarkably good accuracy if the initial parameters are known [16–24].

The second part of this Chapter is therefore dedicated to illustrate how it is possible to predict the spin and mass properties of the black hole produced in a binary merger simply on the basis of the properties of initial black holes. The discussion I will provide does not want to be exhaustive nor complete and some of the most recent work, e.g., [25, 26], will not be presented in detail. Rather, the presentation will be mostly pedagogical and aimed at providing a basic description and a series of references where additional information can be found. In particular, after adopting a specific recipe to describe how to compute such properties via a simple algebraic expression [21, 27], I will explore its predictions in the large space of parameters. All of the considerations made here apply to binary systems that inspiral from very large separations and hence through quasi-circular orbits. Such configurations are the ones more likely to occur astrophysically since any residual eccentricity is lost quickly by the gravitational-radiation reaction. Much of the text in the following has been taken from [25, 27, 28].

### 1.6.1 Modelling the Final Spin

A number of analytical approaches have been developed over the years to determine the final spin from a binary black hole coalescence [29–33]. A first line of research has exploited the motion of test particles in black hole spacetimes [17, 34]. A second approach, instead, has focused on the derivation of analytic expressions which would model the numerical-relativity data but also exploit as much information as possible either from perturbative studies, or from the symmetries of the system when this is in the weak-field limit [16, 18–21, 24, 35–37]. In this sense, these approaches are not blind fits of the data, but, rather, use the numerical-relativity data to construct a physically consistent and mathematically accurate modelling of the final spin.

The common ground shared by these second approaches is in the *assumption* that the final spin vector  $\mathbf{a}_{\text{fin}}$ , when seen as the function  $\mathbf{a}_{\text{fin}} = \mathbf{a}_{\text{fin}}(\mathbf{a}_1, \mathbf{a}_2, \nu)$ , where  $\mathbf{a}_{1,2} = \mathbf{S}_{1,2}/M_{1,2}^2$  are the two dimensionless spin vectors ( $|\mathbf{a}_{1,2}| \in [0, 1]$ ), can be expressed as a Taylor expansion around  $\mathbf{a}_1 = \mathbf{a}_2 = \nu = 0$ . Given that  $|\mathbf{a}_{1,2}| \leq 1$ , this may seem as a mathematically reasonable assumption and the expectation that the series is convergent over the whole space of parameters as a legitimate one. However, this remains an assumption, and different routes have been chosen to constrain the coefficients in the expansion invoking more mathematically-based considerations [18, 23, 24], or more physically-based considerations [16, 20, 21].

Here, however, I will concentrate on reviewing the approach which, with a five physically reasonable assumptions and with five free coefficients to be fixed from the numerical data, leads to a formula that can model generic initial spin configurations and mass ratios, thus covering all of the seven-dimensional space of parameters [16, 20, 21]. In essence, the approach developed in [16, 20, 21, 27]

amounts to considering the dimensionless spin vector of the final black hole as given by the sum of the two initial spins and of a “third” vector parallel to the initial orbital angular momentum when the binaries are widely separated. This “third” vector is an intrinsic “property” of the binary (it will be shown below that this is essentially the orbital angular momentum *not* radiated), thus depending on the initial spin vectors and on the black holes mass ratio, but not on the initial separation. The formula for the final spin then simply describes the properties of this vector in terms of the initial parameters of the binary and of a set of coefficients to be determined from a comparison with numerical simulations.

Let us now consider in more detail how to derive such a formula and consider therefore a generic binary of black holes with masses  $M_1, M_2$ , mass ratio  $q$ , spins  $\mathbf{S}_1, \mathbf{S}_2$  and orbital angular momentum  $\mathbf{L}$ . Let also where  $\alpha, \beta$  and  $\gamma$  be the vector cosines among the different vectors, i.e.,

$$\cos \alpha := \hat{\mathbf{a}}_1 \cdot \hat{\mathbf{a}}_2, \quad \cos \beta := \hat{\mathbf{a}}_1 \cdot \hat{\mathbf{L}}, \quad \cos \gamma := \hat{\mathbf{a}}_2 \cdot \hat{\mathbf{L}}, \quad (1.140)$$

where the “hats” are used to represent unit vectors. A schematic representation of the different vectors and angles is shown in Fig. 1.6.

As mentioned above, five assumptions are needed in order to make the problem tractable analytically and these are listed in what follows. I recall that when the black holes have spins that are aligned with the orbital angular momentum  $\mathbf{L}$ , the numerical-relativity results are accurately described by Rezzolla et al. [21]

$$a_{\text{fin}} = \tilde{a} + \tilde{a}v(s_4\tilde{a} + s_5v + t_0) + v(2\sqrt{3} + t_2v + t_3v^2), \quad (1.141)$$

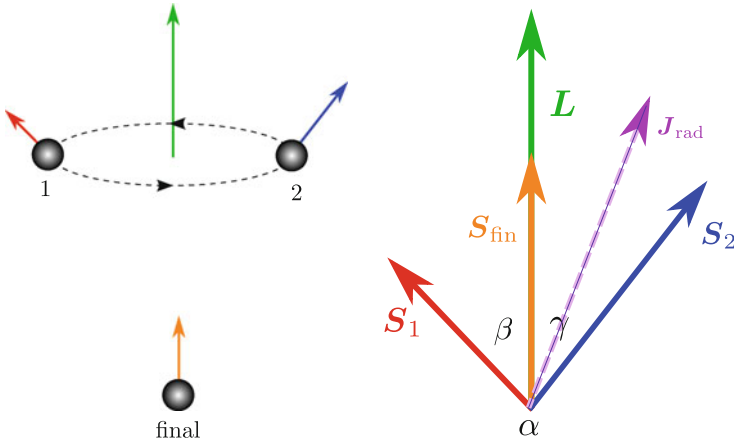


**Fig. 1.6** Schematic representation of the binary system and of the angles between the different spin vectors  $\mathbf{S}_1, \mathbf{S}_2$  and the orbital angular momentum  $\mathbf{L}$ . The dynamics of the binary is summarised on the *left*

where  $\nu := M_1 M_2 / (M_1 + M_2)^2$  is the symmetric mass ratio and  $\tilde{a} := (a_1 + a_2 q^2) / (1 + q^2)$ . The five coefficients  $t_0, t_2, t_3, s_4$  and  $s_5$  in (1.141) can be determined straightforwardly by fitting the results of the numerical-relativity calculations. However, an additional condition can be employed by using the results obtained by Scheel et al. [38] for equal-mass non-spinning black holes and thus enforce that for  $a_1 = a_2 = 0$ ,  $\nu = 1/4$  and to the claimed precision

$$a_{\text{fin}} = \frac{\sqrt{3}}{2} + \frac{t_2}{16} + \frac{t_3}{64} = 0.68646 \pm 0.00004. \quad (1.142)$$

This leaves only *four* unconstrained coefficients, whose value can be fixed by a comparison with numerical-relativity simulations to obtain

$$\begin{aligned} s_4 &= -0.1229 \pm 0.0075, & s_5 &= 0.4537 \pm 0.1463, \\ t_0 &= -2.8904 \pm 0.0359, & t_3 &= 2.5763 \pm 0.4833, \end{aligned} \quad (1.143)$$

with an agreement relative to the numerical-relativity (NR) data  $|a_{\text{fin}}^{\text{NR}} - a_{\text{fin}}^{\text{fit}}| \leq 0.0085$ . Using the constraint (1.142) we then also obtain  $t_2 = -3.5171 \pm 0.1208$ . Note that because expression (1.141) provides information over only 3 of the 7 dimensions of the parameter space, I will next show how to cover the remaining 4 dimensions and thus derive an expression for  $\mathbf{a}_{\text{fin}}$  for *generic* black hole binaries in quasi-circular orbits. Following the spirit of [21, 27], we make the following assumptions:

- (i) *The mass  $M_{\text{rad}}$  radiated to gravitational waves can be neglected* i.e.,  $M_{\text{fin}} = M := M_1 + M_2$ . The radiated mass could be accounted for by using the numerical-relativity data for  $M_{\text{fin}}$  [39] or extrapolating the test-particle behavior [40]. The reason why assumption (i) is reasonable is that  $M_{\text{rad}}$  is largest for aligned binaries, but these are also the ones employed to fit the free coefficients (1.143). Therefore,  $M_{\text{rad}}$  is approximately accounted for by the values of the coefficients. In Section 1.6.3 I will discuss in detail how to estimate  $M_{\text{rad}}$ .
- (ii) *The norms  $|\mathbf{S}_1|$ ,  $|\mathbf{S}_2|$ ,  $|\tilde{\mathbf{I}}|$  do not depend on the binary's separation  $r$* , with  $\tilde{\mathbf{I}}$  being defined as

$$\tilde{\mathbf{I}}(r) := \mathbf{S}_{\text{fin}} - [\mathbf{S}_1(r) + \mathbf{S}_2(r)] = \mathbf{L}(r) - \mathbf{J}_{\text{rad}}(r), \quad (1.144)$$

where  $\mathbf{S}_1(r)$ ,  $\mathbf{S}_2(r)$  and  $\mathbf{L}(r)$  are the spins and the orbital angular momentum at separation  $r$  and  $\mathbf{J}_{\text{rad}}(r)$  is the angular momentum radiated from  $r$  to the merger. Clearly,  $\mathbf{S}_1$ ,  $\mathbf{S}_2$  and  $\tilde{\mathbf{I}}$  can still depend on  $r$  through their directions. While the constancy of  $|\mathbf{S}_1|$  and  $|\mathbf{S}_2|$  is a very good assumption for black holes, which do not have an internal structure, the constancy of  $|\tilde{\mathbf{I}}|$  is more heuristic and based on the idea that the merger takes place at an “effective” innermost stable circular orbit (ISCO), so that  $|\tilde{\mathbf{I}}|$  can be interpreted as the residual orbital angular momentum contributing to  $\mathbf{S}_{\text{fin}}$ .

- (iii) *The final spin  $\mathbf{S}_{\text{fin}}$  is parallel to the initial total angular momentum  $\mathbf{J}(r_{\text{in}}) := \mathbf{S}_1(r_{\text{in}}) + \mathbf{S}_2(r_{\text{in}}) + \mathbf{L}(r_{\text{in}})$ . This amounts to assuming that  $\mathbf{J}_{\text{rad}}(r_{\text{in}}) \parallel \mathbf{J}(r_{\text{in}})$ . It replaces the assumption, made in [21], that  $\mathbf{J}_{\text{rad}}(r_{\text{in}}) \parallel \mathbf{L}(r_{\text{in}})$ , which is only valid for a smaller set of configurations. We note that this assumption is motivated by PN theory: Within the adiabatic approximation, the secular angular-momentum losses via gravitational radiation are along the total angular momentum  $\mathbf{J}$  [41]. This is because as  $\mathbf{L}$  rotates around  $\mathbf{J}$ , the emission orthogonal to  $\mathbf{J}$  averages out. Note that since  $\mathbf{a}_{\text{fin}} \parallel \mathbf{J}(r_{\text{in}})$ , the angle  $\theta_{\text{fin}}$  between the final spin and the initial orbital angular momentum  $\mathbf{L}(r_{\text{in}})$  is given by*

$$\cos \theta_{\text{fin}} = \hat{\mathbf{L}}(r_{\text{in}}) \cdot \hat{\mathbf{J}}(r_{\text{in}}). \quad (1.145)$$

- (iv) *The angle between  $\mathbf{L}$  and  $\mathbf{S} := \mathbf{S}_1 + \mathbf{S}_2$  and the angle between  $\mathbf{S}_1$  and  $\mathbf{S}_2$  are constant during the inspiral, although  $\mathbf{L}$  and  $\mathbf{S}$  precess around  $\mathbf{J}$ .*

At 2.5 PN order, (iii) and (iv) are approximately valid for any mass ratio if only one of the black holes is spinning, and for  $M_1 = M_2$  if one neglects spin-spin couplings. In both cases, in fact,  $\mathbf{S}$  and  $\mathbf{L}$  essentially precess around the direction  $\hat{\mathbf{J}}$ , which remains nearly constant [41], and the angle between the two spins remains constant as well. The only case in which (iii) and (iv) are not even approximately valid is for binaries which, at some point in the evolution, have  $\mathbf{L}(r) \approx -\mathbf{S}(r)$ . These orbits undergo the so-called “transitional precession” [41], as a result of which  $\hat{\mathbf{J}}$  changes significantly. Because transitional precession happens only if  $\mathbf{L}$  and  $\mathbf{S}$  are initially *almost* anti-aligned with  $|\mathbf{L}| > |\mathbf{S}|$ , it affects only a very small region of the parameter space.

- (v) *When the initial spin vectors are equal and opposite and the masses are equal, the spin of the final black hole is the same as for nonspinning binaries. Besides being physically reasonable—reflecting the expectation that if the spins are equal and opposite, their contributions cancel out—this assumption is confirmed by numerical-relativity simulations and by the leading-order PN spin-spin and spin-orbit couplings.*

Making use of these assumptions, it is then possible to derive an expression for the final spin. Let us first use (i) to write (1.144) as

$$\mathbf{a}_{\text{fin}} = \frac{1}{(1+q)^2} (\mathbf{a}_1(r) + \mathbf{a}_2(r)q^2 + \mathbf{l}(r)q), \quad (1.146)$$

where  $\mathbf{a}_{\text{fin}} = \mathbf{S}_{\text{fin}}/M^2$  and  $\mathbf{l} := \tilde{\mathbf{l}}/(M_1M_2)$ . Using (ii), the final-spin norm is

$$|\mathbf{a}_{\text{fin}}| = \frac{1}{(1+q)^2} \left[ |\mathbf{a}_1|^2 + |\mathbf{a}_2|^2 q^4 + 2|\mathbf{a}_2||\mathbf{a}_1|q^2 \cos \alpha + 2(|\mathbf{a}_1| \cos \beta(r) + |\mathbf{a}_2|q^2 \cos \gamma(r)) |\mathbf{l}|q + |\mathbf{l}|^2 q^2 \right]^{1/2}. \quad (1.147)$$

Note that because of the assumption (iv), the angle  $\alpha$  does not depend on the separation and is simply the angle between the spins at the *initial* separation,  $r_{\text{in}}$ , of the numerical-relativity simulations. The angles  $\beta$  and  $\gamma$  are instead functions of the binary's separation, but this dependence cancels out in the linear combination in which they appear in (1.147), which is indeed, within the assumptions made, independent of the separation and which can therefore be evaluated at  $r = r_{\text{in}}$ . To see this, let us consider expression (1.147) at the effective ISCO, that is, a fictitious final separation before the merger takes place. There,  $\mathbf{J}_{\text{rad}}(r_{\text{ISCO}}) = 0$  by definition and therefore  $\mathbf{l}(r_{\text{ISCO}}) = \mathbf{L}(r_{\text{ISCO}})$ . As a result,  $\beta(r_{\text{ISCO}})$  [ $\gamma(r_{\text{ISCO}})$ ] are simply the angles between  $\mathbf{S}_1$  [ $\mathbf{S}_2$ ] and  $\mathbf{L}$  at the ISCO. Using now assumption (iv), we can write part of (1.147) as

$$\begin{aligned} |\mathbf{a}_1| \cos \beta(r_{\text{ISCO}}) + |\mathbf{a}_2| q^2 \cos \gamma(r_{\text{ISCO}}) &= (\hat{\mathbf{L}} \cdot \mathbf{S})_{\text{ISCO}} / M_1^2 \\ &= (\hat{\mathbf{L}} \cdot \mathbf{S}) / M_1^2 = |\mathbf{a}_1| \cos \tilde{\beta}(r) + |\mathbf{a}_2| q^2 \cos \tilde{\gamma}(r), \end{aligned} \quad (1.148)$$

where  $\tilde{\beta}$  and  $\tilde{\gamma}$  are the angles between the spins and  $\mathbf{L}$  at *any separation*  $r$  and thus also at  $r = r_{\text{in}}$

$$\cos \tilde{\beta} := \hat{\mathbf{a}}_1 \cdot \hat{\mathbf{l}}, \quad \cos \tilde{\gamma} := \hat{\mathbf{a}}_2 \cdot \hat{\mathbf{l}}. \quad (1.149)$$

This proves our previous statement: the dependence on  $r$  that  $\beta$  and  $\gamma$  have in expression (1.147) is canceled by the linear combination in which they appear. Stated differently, the final-spin norm is simply given by expression (1.147) where  $\beta(r) \rightarrow \tilde{\beta}(r_{\text{in}})$  and  $\gamma(r) \rightarrow \tilde{\gamma}(r_{\text{in}})$ . Thus, one does not need to worry about the angles between  $\hat{\mathbf{a}}_{1,2}$  and  $\hat{\mathbf{l}}$  but simply about the angles between  $\hat{\mathbf{a}}_{1,2}$  and  $\hat{\mathbf{l}}$  at  $r = r_{\text{in}}$ , which are easy to compute.

Finally, we need to compute  $|\mathbf{l}|$  and for this we proceed like in [21] and match expression (1.147) at  $r = r_{\text{ISCO}}$  with (1.141) for parallel and aligned spins [ $\alpha = \beta(r_{\text{ISCO}}) = \gamma(r_{\text{ISCO}}) = 0$ ], for parallel and antialigned spins [ $\alpha = 0$ ,  $\beta(r_{\text{ISCO}}) = \gamma(r_{\text{ISCO}}) = \pi$ ], and for antiparallel spins which are aligned or antialigned [ $\alpha = \beta(r_{\text{ISCO}}) = \pi$ ,  $\gamma(r_{\text{ISCO}}) = 0$  or  $\alpha = \gamma(r_{\text{ISCO}}) = \pi$ ,  $\beta(r_{\text{ISCO}}) = 0$ ]. As noted in [21], this matching is not unique, but the degeneracy can be broken by exploiting assumption (v) (i.e., by imposing that  $|\mathbf{l}|$  does not depend on  $\mathbf{a}_{1,2}$  when  $\mathbf{a}_1 = -\mathbf{a}_2$  and  $q = 1$ ) and by requiring for simplicity that  $|\mathbf{l}|$  depends linearly on  $\cos \alpha$ ,  $\cos \beta$  and  $\cos \gamma$ . Using these constraints and (1.148) we obtain again an expression valid for *any separation* and hence for  $r = r_{\text{in}}$

$$\begin{aligned} |\mathbf{l}| &= 2\sqrt{3} + t_2 v + t_3 v^2 \\ &+ \frac{s_4}{(1+q^2)^2} (|\mathbf{a}_1|^2 + |\mathbf{a}_2|^2 q^4 + 2|\mathbf{a}_1||\mathbf{a}_2| q^2 \cos \alpha) \\ &+ \left( \frac{s_5 v + t_0 + 2}{1+q^2} \right) (|\mathbf{a}_1| \cos \tilde{\beta}(r_{\text{in}}) + |\mathbf{a}_2| q^2 \cos \tilde{\gamma}(r_{\text{in}})). \end{aligned} \quad (1.150)$$

In summary, the combination of expressions (1.147) and (1.150) provide a simple and algebraic route to compute the properties of the full spin vector of a black hole resulting from the merger of a binary system in quasi-circular orbit.

## 1.6.2 Exploring the Space of Parameters

In what follows I discuss in some detail the predictions of expressions (1.147) and (1.150) for some simple cases and highlight how to extract interesting physical considerations.

### – Unequal mass, aligned/antialigned equal spins –

If the black holes have *unequal mass* but spins that are *equal, parallel* and *aligned/antialigned* with the orbital angular momentum, i.e.,  $|\mathbf{a}_1| = |\mathbf{a}_2| = a$ ,  $\alpha = 0$ ;  $\beta = \gamma = 0, \pi$ , the prediction for the final spin is given by the simple expression (1.141) [20], where  $\cos \beta = \pm 1$  for aligned/antialigned spins. Note that since the coefficients in (1.141) are determined by fits to the numerical data and the latter is scarcely represented at very large spins, the predictions of expression (1.141) for nearly maximal black holes are essentially extrapolations and are therefore accurate to a few percent at most. As an example, when  $a = 1$ , the formula (1.141) is a non-monotonic function with maximum  $a_{\text{fin}} \simeq 1.029$  for  $\nu \simeq 0.093$ ; this clearly is an artefact of the extrapolation.

The global behaviour of the final spin for unequal-mass and aligned/antialigned equal-spin binaries is summarised in Fig. 1.7, which shows the functional dependence of expression (1.141) on the symmetric mass ratio and on the initial spins. Squares refer to numerical-relativity values as reported in [19, 20, 42–46], while circles to the EMRL constraints. A number of interesting considerations can now be made:

- (a) Using expression (1.141) it is possible to estimate that the minimum and maximum final spins for an equal-mass binary are  $a_{\text{fin}} = 0.3502 \pm 0.03$  and  $a_{\text{fin}} = 0.9590 \pm 0.03$ , respectively. While the value for the maximum spin is most likely underestimated the minimum value is expected to be much more accurate than the estimate in [22], which tends to underestimate the final spin for  $a \lesssim -0.3$ .
- (b) Using expression (1.141) it is straightforward to determine the conditions under which the merger will lead to a final *Schwarzschild* black hole. In practice this amounts to requiring  $a_{\text{fin}}(a, \nu) = 0$  and this curve is shown in Fig. 1.8 with a blue dashed line (cf. also the red dashed line in Fig. 1.7). Binaries on the curve produce Schwarzschild black holes, while binaries above the curve start with a positive total angular momentum and end with a positive one; binaries below the curve, on the other hand, start with a positive total angular momentum and end with a negative one, i.e., with a *global flip*. Several numerical simulations have been carried out to validate this condition [20, 46] and all of them have shown to produce black holes with  $a_{\text{fin}} \lesssim 0.01$  (cf. squares in Fig. 1.7 with  $\nu \simeq 0.16$ ).

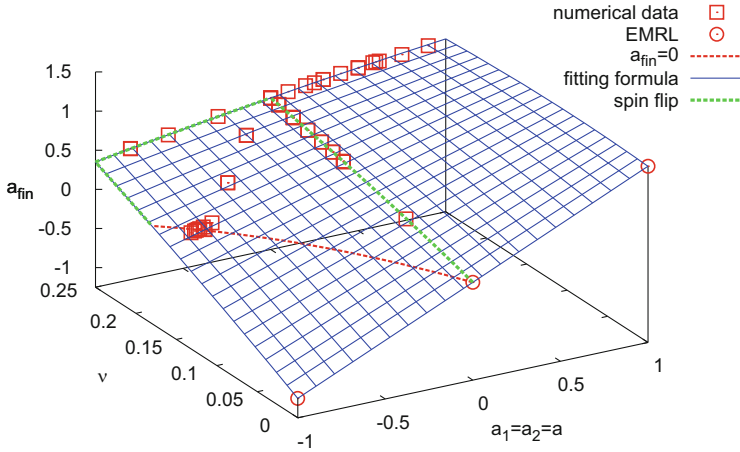


**Fig. 1.7** Global dependence of the final spin on the symmetric mass ratio and on the initial spins as predicted by expression (1.141) for equal-mass, aligned/antialigned equal-spin binaries. *Squares* refer to numerical-relativity values, while *circles* to the extreme mass-ratio limit (EMRL) constraints. Indicated with a *red dashed line* is the locus of points leading to a Schwarzschild black hole (i.e.,  $a_{\text{fin}} = 0$ ), while *green solid lines* mark the region leading to a “spin-flip” (i.e.,  $a_{\text{fin}} < 0$ ) [figure taken from [28]]

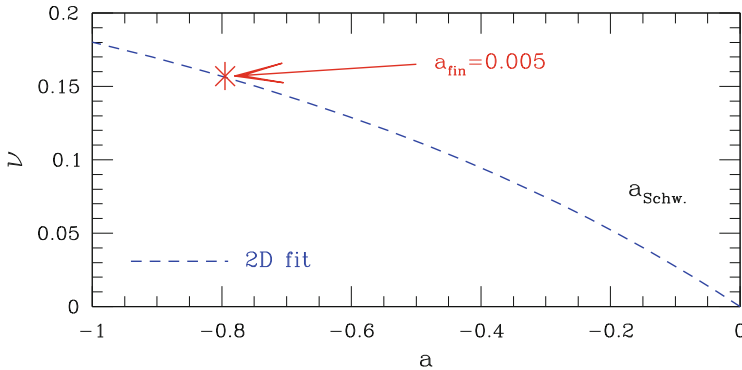
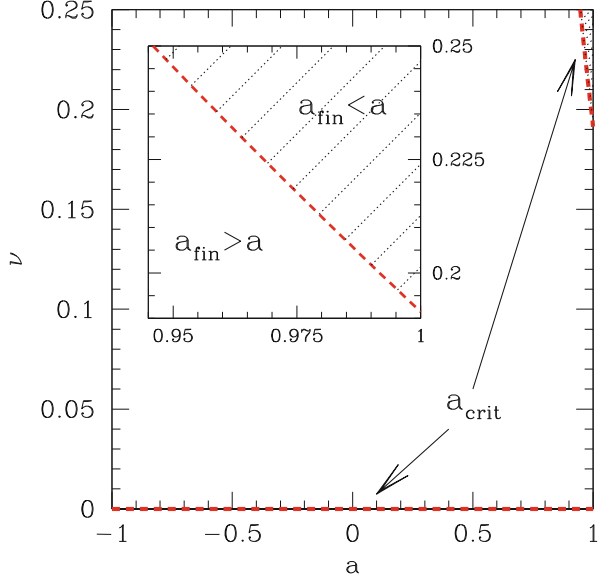


**Fig. 1.8** Set of initial spins and mass ratios leading to a final Schwarzschild black hole: i.e.,  $a_{\text{fin}}(a, \nu) = 0$ . Indicated with a *star* is a numerical example leading to  $a_{\text{fin}} = 0.005$  [figure adapted from [20]]

Overall, the behaviour captured by expression (1.141) shows that in order to produce a nonspinning black hole it is necessary to have unequal-masses (the largest possible mass ratio is  $\nu \simeq 0.18$ ) and spins antialigned with the orbital angular momentum to cancel the contribution of the orbital angular momentum to the total one.

(c) Using expression (1.141) it is also straightforward to determine the conditions under which the merger will lead to a “spin-flip”, namely when the newly

**Fig. 1.9** Critical values of the initial spin and mass ratio leading to a final black hole having the same spin as the initial ones i.e.,  $a_{\text{fin}}(a, \nu) = a$ . A magnification is shown in the inset, where the dashed/non-dashed region refers to binaries spun-down/up by the merger [figure taken from [20]]



formed black hole will spin in the direction opposite to that of the two initial black holes. Mathematically this is equivalent to determine the region in the plane  $(a, \nu)$  such that  $a_{\text{fin}}(a, \nu) a < 0$  and it is shown in Fig. 1.9 as limited by the red dashed line. Overall, it is clear that a spin-flip can take place only for very large mass ratios if the black holes are initially rapidly spinning and that small mass ratios will lead to a spin-flip only for binaries with very small spins.

- (d) Finally, using expression (1.141) it is also possible to determine the conditions under which the merger will lead to a final black hole with the *same* spin as the initial ones. This amounts to requiring that  $a_{\text{fin}}(a, \nu) - a = 0$  and only a very small portion of the  $(a, \nu)$  plane does satisfy this condition (cf. Fig. 5 of [20]). For equal-mass binaries, for instance, the critical value is  $a_{\text{crit}} \gtrsim 0.946$  and no spin-down is possible for  $\nu \lesssim 0.192$ . Because of the minuteness of the region for which  $a_{\text{fin}} < a$ , black holes from aligned-spins binaries are typically *spun-up* by mergers. As it will be shown also in the following Section, this statement is true also for other configurations and is probably true in general.

– *Equal-mass, aligned/antialigned unequal spins* –

Equally interesting is to consider the prediction for the final spin in the case in which the initial black holes have *equal mass* but *unequal* spins that are either *parallel* or *antiparallel* to the orbital angular momentum, i.e., for  $q = 1$  and  $\alpha = 0, \pi; \beta = 0, \pi; \gamma = 0, \pi$ . Setting  $2|\mathbf{a}_1| \cos \beta = a_1 + a_2$  in expression (1.147) we obtain the simple expression for the final spin in these cases [16]

$$a_{\text{fin}}(a_1, a_2) = p_0 + p_1(a_1 + a_2) + p_2(a_1 + a_2)^2, \quad (1.151)$$

where the coefficients  $p_0, p_1$  and  $p_2$  are given by

$$p_0 = \frac{\sqrt{3}}{2} + \frac{t_2}{16} + \frac{t_3}{64} \simeq 0.6869, \quad p_1 = \frac{1}{2} + \frac{s_5}{32} + \frac{t_0}{8} \simeq 0.1522, \quad (1.152)$$

$$p_2 = \frac{s_4}{16} \simeq -0.0081. \quad (1.153)$$

Note that the coefficients  $p_0, p_1, p_2$  and  $s_4, s_5, t_0, t_2, t_3$  were obtained through independent fits of two distinct data sets. The fact they satisfy the conditions (1.152) within the expected error-bars is an important consistency check.

When seen as a power series of the initial spins, expression (1.151) suggests an interesting physical interpretation. Its zeroth-order term,  $p_0$ , can be associated with the (dimensionless) orbital angular momentum not radiated in gravitational waves and thus amounting to  $\sim 70\%$  of the final spin at most. Interestingly, the value for  $p_0$  is in very good agreement with what is possibly the most accurate measurement of the final spin from this configuration and that has been estimated to be  $a_{\text{fin}} = 0.68646 \pm 0.00004$  [47]. Similarly, the first-order term in (1.151),  $p_1$ , can be seen as the contributions from the initial spins and from the spin-orbit coupling, amounting to  $\sim 30\%$  of the final spin at most. Finally, the second-order term,  $p_2$ , can be seen as accounting for the spin-spin coupling, with a contribution to the final spin which is of  $\sim 4\%$  at most.

Another interesting consideration is possible for equal-mass binaries having spins that are equal and antiparallel, i.e.,  $q = 1$ ,  $\mathbf{a}_1 = -\mathbf{a}_2$ . In this case, expressions (1.147) and (1.150) reduce to

$$|\mathbf{a}_{\text{fin}}| = \frac{|\mathbf{l}|}{4} = \frac{\sqrt{3}}{2} + \frac{t_2}{16} + \frac{t_3}{64}. \quad (1.154)$$

Because for equal-mass black holes which are either nonspinning or have equal and opposite spins, the vector  $\mathbf{l}$  does not depend on the initial spins, expression (1.154) states that  $|\mathbf{l}|M_{\text{fin}}^2/4 = |\mathbf{l}|M^2/4 = |\mathbf{l}|M_1M_2$  is, for such systems, the orbital angular momentum at the effective ISCO. We can take this a step further and conjecture that  $|\mathbf{l}|M_1M_2$  is the series expansion of the dimensionless orbital angular momentum at the ISCO also for *unequal-mass* binaries which are either nonspinning or with equal and opposite spins. The zeroth-order term of this series (namely, the term  $2\sqrt{3}M_1M_2$ ) is exactly the one predicted from the EMRL.

– *Generic (misaligned) binaries: unequal mass, unequal spins* –

When the binaries are generic, namely when the initial spins are oriented in generic directions and the two masses are different, the spin expressions (1.147), (1.150) does not reduce to a simple expression and the analysis of the physical implications becomes more complex.

Much more challenging is also the numerical solution in these cases, partly because they are computationally more expensive (no symmetries can be exploited to reduce the computational domain), and partly because the evolutions start at a

finite separation which does not account for the earlier evolution of the orbital angular momentum vector and of the spins (both of which precess). In addition, because the final spin is oriented in directions which are in principle arbitrarily far from the main coordinate lines, the calculation of the inclination angle from the properties of the final apparent horizon is often non-trivial and suitable definitions need to be introduced (see, e.g., [42]). Overall, however, expressions (1.147), (1.150) are able to capture the behaviour of numerical-relativity calculations with errors that are  $\lesssim 1\%$ .

### 1.6.3 Modelling the Final Mass

In this final Section I will describe briefly another algebraic expression that has been derived to compute the energy radiated in gravitational waves and hence the final mass of the black hole [25]. It is useful to start recalling that when deriving a simple algebraic formula that expresses, with a given precision, the mass/energy radiated by a binary system of black holes, two regimes are particularly well-understood. On the analytic side, in fact, the test-particle limit yields predictions that are well-known and simple to derive. On the numerical side, the simulations of binaries with equal-masses and spins aligned or antialigned with the orbital angular momentum are comparatively simpler to study, and have been explored extensively over the last few years. Hence, it is natural that any attempt to derive an improved expression for the radiated energy should try and match both of these regimes.

Let us therefore start by considering the test-particle limit and, in particular, a Kerr spacetime with mass  $M_1$  and spin parameter  $a := S_1/M_1^2$ , and a particle (or small black hole) with mass  $M_2$  on a equatorial circular orbit with radius  $r \gg M_1$ .<sup>5</sup> To first approximation (i.e., for mass ratios  $q := M_2/M_1 \ll 1$ ), the particle will inspiral towards the black hole under the effect of gravitational-wave emission, moving slowly (“adiabatically”) through a sequence of equatorial circular orbits until it reaches the innermost stable circular orbit (ISCO), where it starts plunging, eventually crossing the horizon. The energy  $E_{\text{rad}}$  emitted by the particle during the inspiral from  $r \gg M_1$  to the moment it merges with the central black hole can be written as

$$\frac{E_{\text{rad}}}{M} = [1 - \tilde{E}_{\text{ISCO}}^{\text{eq}}(a)] v + o(v), \quad (1.155)$$

$$\tilde{E}_{\text{ISCO}}^{\text{eq}}(a) = \sqrt{1 - \frac{2}{3\tilde{r}_{\text{ISCO}}^{\text{eq}}(a)}}, \quad (1.156)$$

$$\tilde{r}_{\text{ISCO}}^{\text{eq}}(a) = r_{\text{ms},\pm}, \quad (1.157)$$

---

<sup>5</sup>Without loss of generality, we can assume that the particle moves on a prograde orbit (i.e. in the positive- $\phi$  direction), and let the spin of the Kerr black hole point up ( $a > 0$ ) or down ( $a < 0$ ).

where  $\tilde{r}_{\text{ISCO}}^{\text{eq}}(a)$  is the equatorial marginally stable circular orbit around a Kerr black hole and thus its expression is the same as in (1.136).

Here,  $\tilde{E}_{\text{ISCO}}$  and  $\tilde{r}_{\text{ISCO}}$  are respectively the energy per unit mass at the ISCO and the ISCO radius in units of  $m_1$ , while the remainder,  $o(\nu)$ , contains the higher-order corrections to the radiated energy.<sup>6</sup> These corrections account, for instance, for the conservative self-force effects, which affect the ISCO position and energy, but also for the deviations from adiabaticity, which arise because of the finiteness of the mass  $m_2$  and which blur the sharp transition between inspiral and plunge, and, more in general, for the energy emitted during the plunge and merger phases.

If the particle is initially on an inclined (i.e., non-equatorial) circular orbit, gravitational-wave emission will still cause it to adiabatically inspiral through a sequence of circular orbits. Also, the inclination of these orbits relative to the equatorial plane, which can be defined as [48]<sup>7</sup>

$$\cos(\iota) := \frac{L_z}{\sqrt{Q + L_z^2}}, \quad (1.158)$$

with  $Q$  and  $L_z$  being respectively the Carter constant and the azimuthal angular momentum, will remain approximately constant during the inspiral [48, 49]. As in the equatorial case, the particle plunges when it reaches the ISCO corresponding to its inclination  $\iota$ . Unlike in the equatorial case, though, the radius of the ISCO as a function of  $a$  and  $\iota$  can only be found numerically. An analytical expression, however, can be derived if one considers only the spin-orbit coupling of the particle to the Kerr black hole, i.e., if one considers small spins  $a \ll 1$ . In that case, in fact, one can explicitly check [using, for instance, equations (4)–(5) of [49]] that the ISCO location and energy depend only on the combination  $a \cos(\iota)$ , so that at  $\mathcal{O}(a)^2$ , the generalisation of expressions (1.155)–(1.157) to inclined orbits is given by

$$\frac{E_{\text{rad}}}{M} = [1 - \tilde{E}_{\text{ISCO}}(a, \iota)] \nu + o(\nu), \quad (1.159)$$

$$\tilde{E}_{\text{ISCO}}(a, \iota) \approx \sqrt{1 - \frac{2}{3\tilde{r}_{\text{ISCO}}(a, \iota)}}, \quad (1.160)$$

$$\tilde{r}_{\text{ISCO}}(a, \iota) \approx \tilde{r}_{\text{ISCO}}^{\text{eq}}(a \cos(\iota)), \quad (1.161)$$

where  $\tilde{r}_{\text{ISCO}}^{\text{eq}}$  is given by (1.157). Expressions (1.159)–(1.161) reduce to Eqs. (1.155)–(1.157) in the case of equatorial orbits ( $\iota = 0$ ) and are therefore exact in that limit, with the exception of the higher-order terms in  $\nu$ .

<sup>6</sup>I here use the Landau symbol  $o$ , so that  $f = o(g)$  indicates that  $f/g \rightarrow 0$  when  $g \rightarrow 0$ . Similarly, we will also use the Landau symbol  $\mathcal{O}$ , where instead  $f = \mathcal{O}(g)$  indicates that  $f/g \rightarrow \text{const}$  when  $g \rightarrow 0$ .

<sup>7</sup>As in the equatorial case, we can consider only prograde orbits ( $0 \leq \iota \leq \pi/2$ ) and allow  $a$  to be either positive or negative.

As mentioned above, another case in which we know accurately the total energy emitted in gravitational waves is given by binaries of black holes with equal masses and spins aligned or antialigned with the orbital angular momentum. Reisswig et al. [50], for instance, showed that the energy emitted by these binaries during their inspiral (from infinite separation), merger and ringdown can be well described by a polynomial fit [25, 50]

$$\frac{E_{\text{rad}}}{M} = w_0 + w_1(a_1 + a_2) + \frac{w_1}{4}(a_1 + a_2)^2, \quad (1.162)$$

where the fitting coefficients were found to be [25]

$$w_0 = 0.04827 \pm 0.00039, \quad w_1 = 0.01707 \pm 0.00032, \quad (1.163)$$

I recall that the coefficient  $w_0$  can be interpreted as the nonspinning orbital contribution to the energy loss (which is the largest one and  $\sim 50\%$  of the largest possible mass loss, which happens for  $a_1 = a_2 = 1$ ),  $w_1$  can instead be interpreted as the spin-orbit contribution (which is  $\lesssim 30\%$  of the largest possible loss), while  $w_1/4$  can be associated to the spin-spin contribution (which is  $\lesssim 20\%$  of the largest possible loss). Expression (1.162) reproduces all of the available numerical-relativity data for the energy emitted by equal-mass binaries with aligned or antialigned spins, to within  $\sim 0.005M$  (except for almost maximal spins). Note, however, that higher-order terms in the spins may be needed in Eq. (1.162) to reproduce the data for nearly extremal spins.

Using therefore the knowledge of the radiated energy from the test-particle limit and from the equal-mass aligned/antialigned configurations, it is possible to derive an expression valid for generic binaries. As a first step, let us note that the PN binding energy of an equal-mass binary of spinning black holes depends on the spins, at 1.5 PN order, i.e., at leading order in the spins, only through the combination

$$\frac{\hat{\mathbf{L}} \cdot (\mathbf{S}_1 + \mathbf{S}_2)}{M^2} = \frac{|\mathbf{a}_1| \cos \beta + |\mathbf{a}_2| \cos \gamma}{4}. \quad (1.164)$$

One can therefore attempt to extend expression (1.162) to generic equal-mass binaries simply by replacing  $a_1 + a_2$  with  $|\mathbf{a}_1| \cos \beta + |\mathbf{a}_2| \cos \gamma$ , i.e., obtaining

$$\begin{aligned} \frac{E_{\text{rad}}}{M} &= w_0 + w_1(|\mathbf{a}_1| \cos \beta + |\mathbf{a}_2| \cos \gamma) \\ &\quad + \frac{w_1}{4}(|\mathbf{a}_1| \cos \beta + |\mathbf{a}_2| \cos \gamma)^2. \end{aligned} \quad (1.165)$$

Because in the test-particle limit the angle  $\beta$  becomes the angle between the spin  $\mathbf{S}_1$  of the Kerr black hole and the orbital angular momentum of the particle, thus

coinciding with the angle  $\iota$  defined in (1.158), it is natural to rewrite Eqs. (1.159)–(1.161) as

$$\frac{E_{\text{rad}}}{M} = [1 - \tilde{E}_{\text{ISCO}}(\tilde{a})] \nu + o(\nu), \quad (1.166)$$

$$\tilde{E}_{\text{ISCO}}(\tilde{a}) = \sqrt{1 - \frac{2}{3\tilde{r}_{\text{ISCO}}^{\text{eq}}(\tilde{a})}}, \quad (1.167)$$

where we have defined

$$\tilde{a} := \frac{\hat{\mathbf{L}} \cdot (\mathbf{S}_1 + \mathbf{S}_2)}{M^2} = \frac{|\mathbf{a}_1| \cos \beta + q^2 |\mathbf{a}_2| \cos \gamma}{(1 + q)^2}. \quad (1.168)$$

If we now assume that the higher-order term  $o(\nu)$  in Eq. (1.166) is quadratic in  $\nu$ , we can determine it by imposing that we recover the equal-mass expression (1.165) for  $q = 1$ , thus obtaining the final expression

$$\begin{aligned} \frac{E_{\text{rad}}}{M} &= [1 - \tilde{E}_{\text{ISCO}}(\tilde{a})] \nu \\ &+ 4\nu^2 [4w_0 + 16w_1 \tilde{a}(\tilde{a} + 1) + \tilde{E}_{\text{ISCO}}(\tilde{a}) - 1], \end{aligned} \quad (1.169)$$

where  $\tilde{E}_{\text{ISCO}}(\tilde{a})$  is given by (1.167). By construction, therefore, expression (1.169) has the correct behavior both in the test-particle limit and for equal-mass binaries. It should be noted that the fitting coefficients [given by (1.163)] are obtained using only a subset of the numerical-relativity data, that is, those for equal-mass binaries with *aligned/antialigned* spins. Yet, expression (1.169) is in reasonable agreement with all the published data, both at large and small separations. This is best seen in Fig. 1.10, where we plot the final mass of the remnant for all the published data for binaries with  $a_1 \cos \beta = a_2 \cos \gamma$  (blue circles), as well as the predictions of our expression when applied to the “small-separation” initial data of the simulations (meshed surface). Clearly, spinning binaries with unequal mass ratios are essentially absent, and simulations for such binaries will provide a very significant check of our expression (1.169). Nevertheless, the simple functional dependence shown by the available data, whose behaviour can be well captured with low-order polynomials is quite remarkable.

The graphical representation of the data in Fig. 1.10 highlights that the largest radiated energy,  $E_{\text{rad}}(a = 1)/M = 9.95\%$ , is lost by binaries with equal-mass and maximally spinning black holes with spins aligned with the orbital angular momentum. Hence, black-hole binaries on quasi-circular orbits are among the most efficient sources of energy in the universe. Note, however, that equal-mass binaries are not always the systems that lose the largest amount of energy. Indeed, unequal-mass systems with sufficiently large spins aligned with the angular momentum can lead to emissions larger than those from equal-mass binaries but with large antialigned spins. For instance, a binary with  $\nu = 0.15$  and  $a_1 = a_2 = 1$  will

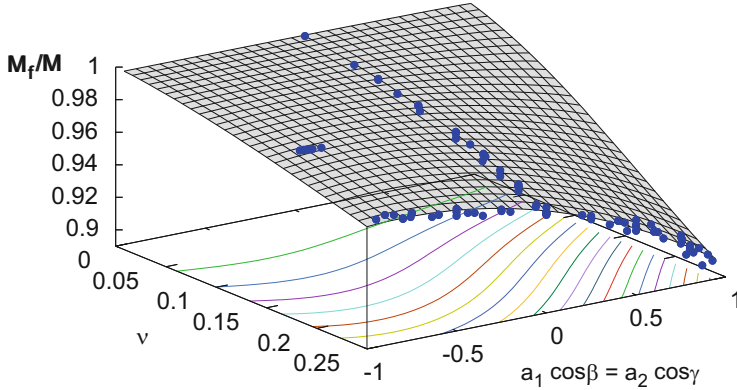


**Fig. 1.10** Mass of the final black hole,  $M_f \equiv M - E_{\text{rad}}$ , and corresponding fit for all the published binaries with  $a_1 \cos \beta = a_2 \cos \gamma$ . Note the simple functional dependence of the  $E_{\text{rad}}$ , whose behaviour can be well captured with low-order polynomials

radiate more than a binary with  $\nu = 0.25$  and  $a_1 = -a_2$ . This is simply due to the interplay of the last two terms in expression (1.169).

**Acknowledgements** It is a pleasure to thank the organizers of a very interesting school. I am grateful go to Francesco Haardt, Ugo Moschella, and Vittorio Gorini for their invaluable help in transforming my scattered hand-written notes into something readable.

## References

1. Rezzolla, L., Zanotti, O.: *Relativistic Hydrodynamics*. Oxford University Press, Oxford (2013)
2. Misner, C.W., Thorne, K.S., Wheeler, J.A.: *Gravitation*. Freeman, New York (1974)
3. Schutz, B.F.: *An Introduction to General Relativity*. Cambridge University Press, Cambridge (1984)
4. d’Inverno, R.: *Introducing Einstein’s Relativity*. Oxford University Press, Oxford (1990)
5. Chandrasekhar, S.: *The Mathematical Theory of Black Holes*. Oxford University Press, Oxford UK (1992)
6. Oppenheimer, J.R., Snyder, H.: *Phys. Rev. D* **56**, 455 (1939)
7. Font, J.A., Goodale, T., Iyer, S., Miller, M., Rezzolla, L., Seidel, E., Stergioulas, N., Suen, W.-M., Tobias, M.: *Phys. Rev. D* **65**, 084024 (2002)
8. Baiotti, L., Hawke, I., Montero, P., Loeffler, F., Rezzolla, L., Stergioulas, N., Font, T., Seidel, E.: *Phys. Rev. D* **71**, 024035 (2005)
9. Baiotti, L., Hawke, I., Rezzolla, L.: *Class. Quantum Gravity* **24**, S187 (2006)
10. Baiotti, L., Rezzolla, L.: *Phys. Rev. Lett.* **97**, 141101 (2006)
11. Baiotti, L., Hawke, I., Rezzolla, L., Schnetter, E.: *Phys. Rev. Lett.* **94**, 131101 (2005)
12. Kerr, R.P.: *Phys. Rev. Lett.* **11**, 237 (1963)
13. Pretorius, F.: *Phys. Rev. Lett.* **95**, 121101 (2005)
14. Campanelli, M., Lousto, C.O., Marronetti, P., Zlochower, Y.: *Phys. Rev. Lett.* **96**, 111101 (2006)

15. Baker, J.G., Centrella, J., Choi, D.I., Koppitz, M., van Meter, J.: Phys. Rev. D **73**, 104002 (2006)
16. Rezzolla, L., Dorband, E.N., Reisswig, C., Diener, P., Pollney, D., Schnetter, E., Szilágyi, B.: Astrophys. J. **708**, 1422 (2007)
17. Buonanno, A., Kidder, L.E., Lehner, L.: Phys. Rev. D **77**, 026004 (2008)
18. Boyle, L., Kesden, M.: Phys. Rev. D **78**, 024017 (2008)
19. Marronetti, P., Tichy, W., Bruegmann, B., Gonzalez, J., Sperhake, U.: Phys. Rev. D **77**, 064010 (2008)
20. Rezzolla, L., Diener, P., Dorband, E.N., Pollney, D., Reisswig, C., Schnetter, E., Seiler, J.: Astrophys. J. **674**, L29 (2008)
21. Rezzolla, L., Barausse, E., Dorband, E.N., Pollney, D., Reisswig, C., Seiler, J., Husa, S.: Phys. Rev. D **78**, 044002 (2008)
22. Kesden, M.: Phys. Rev. D **78**, 084030 (2008)
23. Tichy, W., Marronetti, P.: Phys. Rev. D **78**, 081501 (2007)
24. Boyle, L., Kesden, M., Nissanke, S.: Phys. Rev. Lett. **100**, 151101 (2008)
25. Barausse, E., Morozova, V., Rezzolla, L.: Astrophys. J. **756**, 63 (2012)
26. Healy, J., Lousto, C.O., Zlochower, Y.: Phys. Rev. D **90**, 104004 (2014)
27. Barausse, E., Rezzolla, L.: Astrophys. J. **704**, L40 (2009)
28. Rezzolla, L.: Class. Quantum Gravity **26**, 094023 (2009)
29. Buonanno, A., Damour, T.: Phys. Rev. D **62**, 064015 (2000)
30. Damour, T.: Phys. Rev. D **64**, 124013 (2001)
31. Buonanno, A., Chen, Y., Damour, T.: Phys. Rev. D **74**, 104005 (2006)
32. Damour, T., Nagar, A.: Phys. Rev. D **76**, 044003 (2007)
33. Gergely, L.A., Biermann, P.L.: J. Phys. Conf. Ser. **122**, 012040 (2008)
34. Hughes, S.A., Blandford, R.D.: Astrophys. J. **585**, L101 (2003)
35. Campanelli, M., Lousto, C.O., Zlochower, Y.: Phys. Rev. D **74**, 041501 (2006)
36. Campanelli, M., Lousto, C.O., Zlochower, Y.: Phys. Rev. D **74**, 084023 (2006)
37. Campanelli, M., Lousto, C.O., Zlochower, Y.: Phys. Rev. D **73**, 061501(R) (2006)
38. Scheel, M.A., Boyle, M., Chu, T., Kidder, L.E., Matthews, K.D., Pfeiffer, H.P.: Phys. Rev. D **79**, 024003 (2009)
39. Tichy, W., Marronetti, P.: Phys. Rev. D **78**, 081501 (2008)
40. Kesden, M.: Phys. Rev. D **78**, 084030 (2008)
41. Apostolatos, T.A., Cutler, C., Sussman, G.J., Thorne, K.S.: Phys. Rev. D **49**, 6274 (1994)
42. Campanelli, M., Lousto, C.O., Zlochower, Y., Krishnan, B., Merritt, D.: Phys. Rev. D **75**, 064030 (2007)
43. Berti, E., Cardoso, V., Gonzalez, J.A., Sperhake, U., Hannam, M., Husa, S., Brüggmann, B.: Phys. Rev. D **76**, 064034 (2007)
44. Buonanno, A., et al.: Phys. Rev. D **76**, 104049 (2007)
45. Gonzalez, J.A., Sperhake, U., Bruegmann, B.: Phys. Rev. D **79**, 124006 (2009)
46. Berti, E., Cardoso, V., Gonzalez, J.A., Sperhake, U., Bruegmann, B.: Class. Quantum Gravity **25**, 114035 (2008)
47. Scheel, M.A., Boyle, M., Chu, T., Kidder, L.E., Matthews, K.D., Pfeiffer, H.P.: Phys. Rev. D **79**, 024003 (2008)
48. Hughes, S.A.: Phys. Rev. D **64**, 064004 (2001)
49. Barausse, E., Hughes, S.A., Rezzolla, L.: Phys. Rev. D **76**, 044007 (2007)
50. Reisswig, C., Husa, S., Rezzolla, L., et al.: Phys. Rev. D **80**, 124026 (2009)